LAPPEENRANTA-LAHTI UNIVERSITY OF TECHNOLOGY LUT
School of Energy Systems
Electrical Engineering

Dmitrii Shumilin

DEVELOPMENT OF LOW-POWER HIGH-SPEED TURBOGENERATOR

Examiners: Professor Juha Pyrhönen
D.Sc. Ilya Petrov

ABSTRACT

Lappeenranta-Lahti University of Technology LUT
School of Energy Systems
Electrical Engineering

Dmitrii Shumilin

Development of low-power high-speed turbogenerator

Master's thesis

2021
83 pages, 55 figures, 2 tables and 2 appendices

Examiners: Professor Juha Pyrhönen and D.Sc. Ilya Petrov

Keywords: ORC cycle, gas-dynamic stand, turbogenerator, permanent magnet synchronous generator, microturbine, mechanical strength.

Mankind always needs heat and electricity. Renewable energy sources utilized via organic Rankine cycle (ORC) which use turbogenerators as a power machine belonging to sustainably developing areas in the energy sector. ORC plants use waste heat, pellet fuel, or waste as primary sources of energy. Full-scale development of such machines is hampered by the high cost of equipment for implementing the cycle and iterative revision of the turbogenerator.

This work proposes to carry out model experiments over machines on the gas-dynamic test stands. A roadmap for designing an experimental high-speed low-power turbogenerator is presented. A turbogenerator with a rotational speed of 150 000 rpm and a power of 1 kW has been studied from electromagnetism, fluid dynamics, and mechanics' points of view.

ACKNOWLEDGEMENTS

This master's degree was written at the Lappeenranta University of Technology in 2021 during my double degree program.

I would like to express my appreciation to my academic supervisors Professor Juha Pyrhönen from LUT University and Professor Michael Rumyantsev from MPEI University. I also would like to thank my examiner Ilya Petrov and consultant Alexey Sizyakin for their help in completing and writing this work.

I express special gratitude to my family Shumilin Alexey, Shumilina Elena, Shumilin Daniil for their support along this way.

Dmitrii Shumilin
Lappeenranta 18.04.2021

Table of contents

List of symbols and abbreviations

B	Magnetic flux density	T
B_m	Magnetic flux density amplitude close to magnet	T
B_r	Remanence	T
BH_{max}	Maximum energy product	J/m^3
C_f	Fictitious flow speed	m/s
d_m	Diameter of magnet	m
F	Magnetic voltage	A
F_{dem}	Demagnetizing magnetic voltage	A
f	Frequency	Hz
$f1$	First natural frequency of oscillations	Hz
$f2$	Second natural frequency of oscillations	Hz
$f3$	Third natural frequency of oscillations	Hz
G	Mass flow rate	kg/s
g	Gravitational constant of Earth	9.81 m/s^2
H_c	Coercive force	A/m
H_{dem}	Demagnetizing magnetic strength	A/m
k	Line number multiple of the disturbing frequency	-
m	Number of phases	-
n	Rotation speed	rpm
n_0	Nominal rotation speed	rpm
n_s	Specific speed	-
P_0	Inlet pressure to the machine	Pa
p	Number of pole pairs	-
p_{diff}	Pressure difference	Pa
Q	Volume flow rate	m$^{3\cdot}$/s
q	Number of slots per pole and phase	-

r_{pm}	Outer radius of permanent magnet	m
v_d	Peripheral speed at the mean diameter	m/s
x	Coordinate	m
δ	Air gap length	m
μ	Relative air permeability	-
μ_0	Vacuum permeability	$1.256 \cdot 10^{-6}$ H/m
v_{pm}	Poisson's ratio for permanent magnet	-
ρ	Gas density	kg/m^3
ρ_{pm}	Permanent magnet material density	kg/m^3
σ_r	Radial stress	Pa
$\sigma_{r\ press}$	Radial stress from shrink fitting	Pa
Ω	Rotation angular velocity	rad/s

3D	Three dimensional
AC	Alternating current
CAPEX	Capital expenditure
CHP	Combined heat and power
DC	Direct current
EU	European Union
ERI RAS	Energy Research Institute of the Russian Academy of Sciences
FEM	Finite element method
OPEX	Operating expense
ORC	Organic Rankine cycle

PM	Permanent magnet
RES	Renewable energy sources

1 Introduction

1.1 Current state of small-scale power generation unit

Low-power generation systems are based on different renewable energy sources. According to the plot, reproduced from the Eurostat report [1] shown in Figure 1, there has been a clear increasing trend in electricity generation from renewable energy sources (RES) over the past few years.

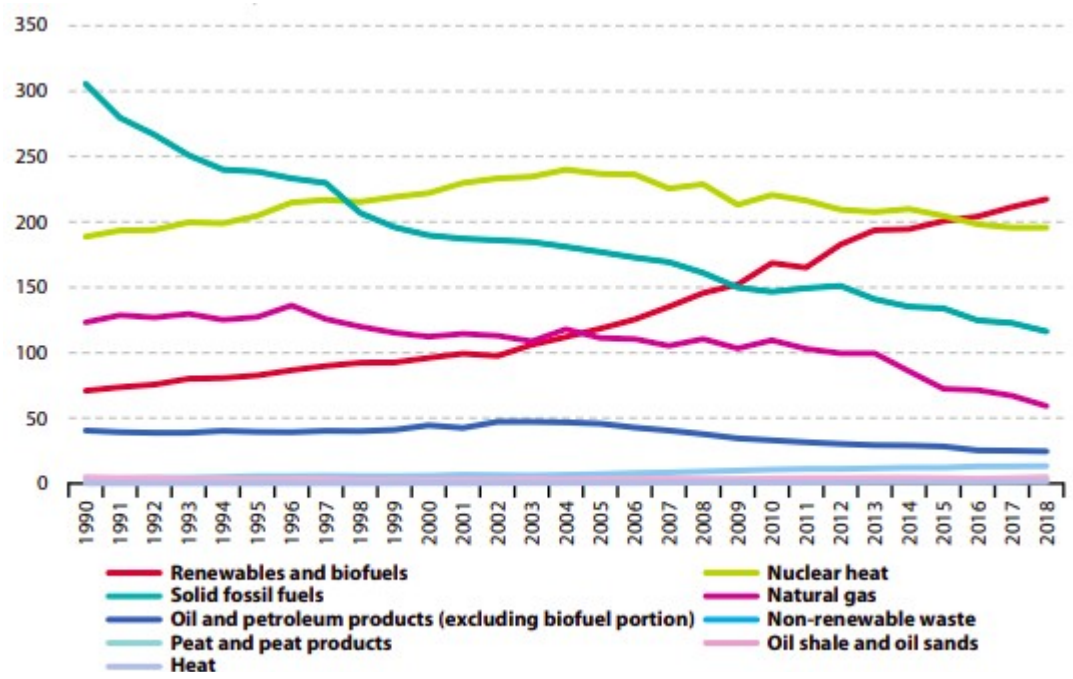

Figure 1: Primary energy production by fuel, EU-27, 1990-2018, (million tonnes of oil equivalent) [1]

Renewable energy now accounts for a significant share of electricity generation in the EU, and even in the last few years, the volume of annual renewable electricity generated has begun to exceed the amount of energy generated by nuclear power plants. Compared to 2017, the amount of renewable energy in 2018 increased up to 34.2 %, and the amount of non-renewable waste energy increased up to 2.1 % in total energy production. According to the report [1], the contribution of various types of energy generation is marked in Figure 2. In the plot, it is possible to conclude that the most voluminous market for renewable energy sources is generating units operating on biofuels, utilization of human or industrial waste, as well as waste heat for various types of production processes.

According to [2], referring to the strategies of Europe until 2050, the renewable energy market will develop at a rapid pace. By 2030, at least 32 % of all energy must be generated by using renewable energy sources.

The Russian energy market has a similar direction of development. According to the forecasts of ERI RAS [3] with any of the approaches to forecasting the development of the energy market the share of installed capacity of RES in Russia will only increase (Figure 3).

Figure 4 shows the prediction of the growth in the use of renewable energy resources in Russia. It can be seen, that solar power market and the market based on biofuels, waste disposal, and waste heat will receive higher development.

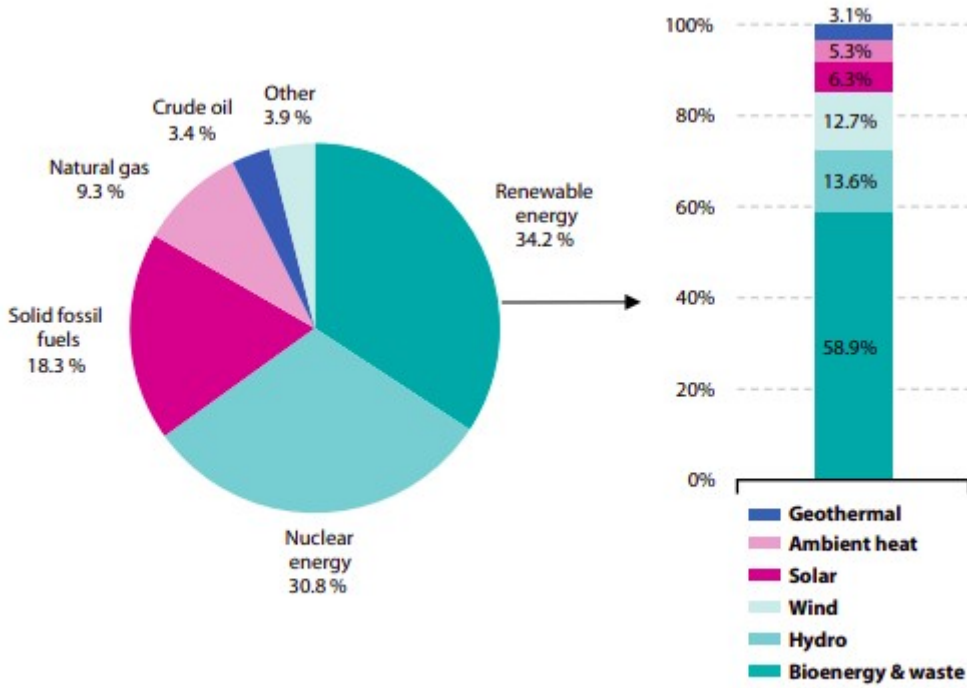

Figure 2: Primary energy sources, EU-27, 2018 (% of total, based on tonnes of oil equivalent) [1]

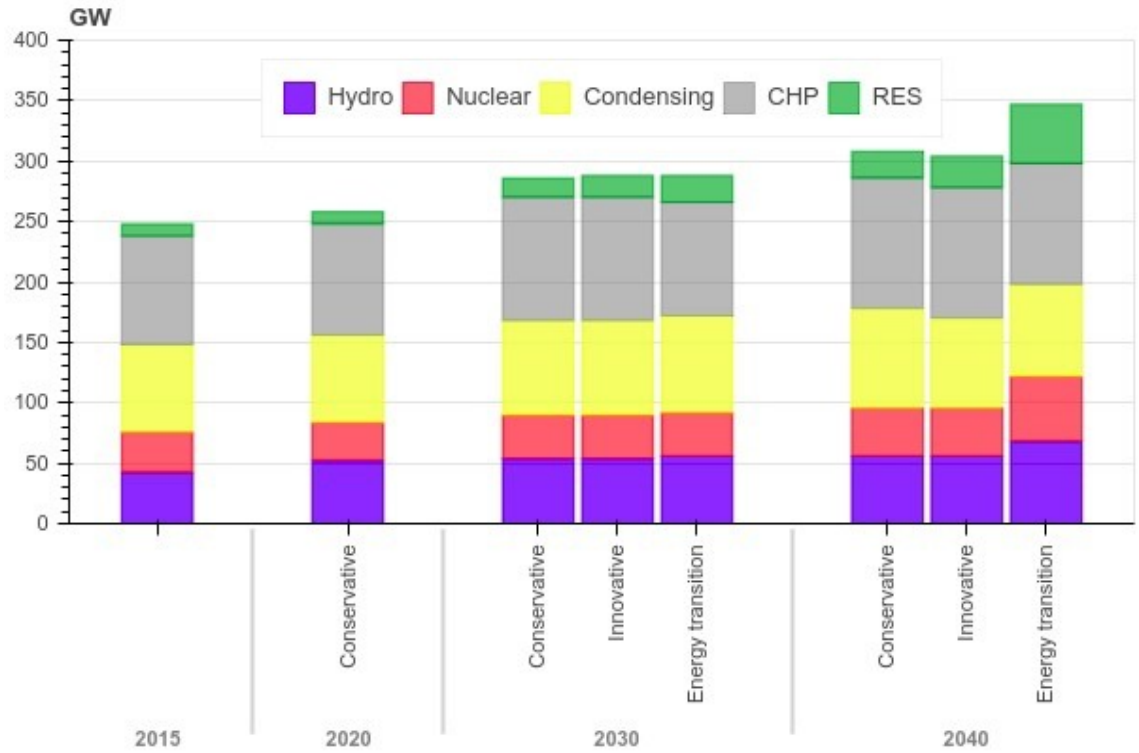

Figure 3: Scenario forecast of the established capacity of the main types of power plants, in GW. [3] (CHP – combined heat and power plant, RES – renewable energy sources, Condensing – Condensing power plants)

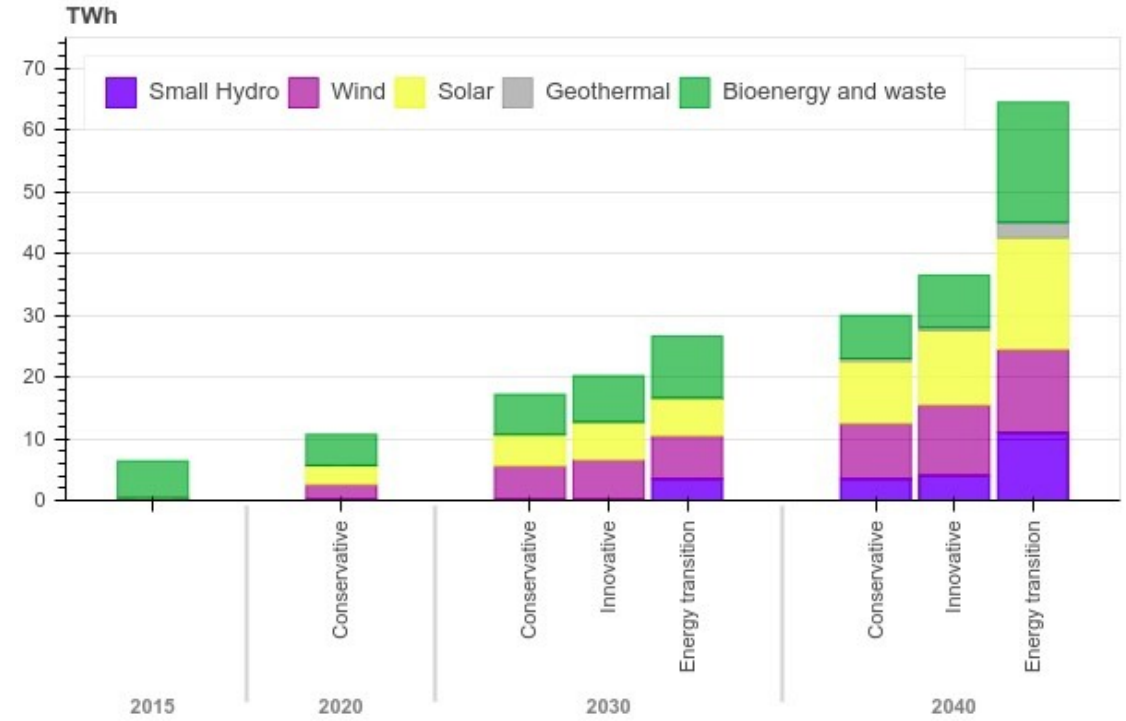

Figure 4: The use of renewable sources in electric power industry, in TWh [3]

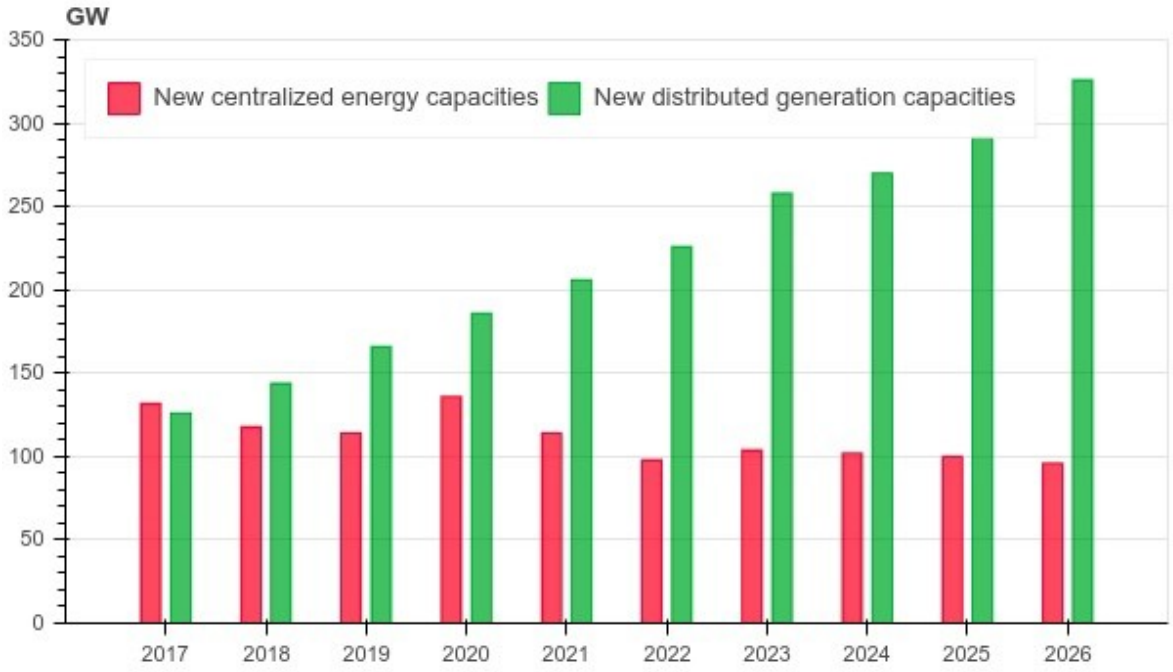

Figure 5: Navigant Research and ERI RAS forecast on the volume of commissioning of distributed generation capacities [3]

Modern trends in the energy sector are largely determined by an increase in the share of decentralized energy supply systems and distributed generation systems. According to the forecast of Navigant Research and ERI RAS (Figure 5), by 2026 the commissioning of new distributed generation capacities in the world will exceed the commissioning of centralized generation capacities [3]. The presented trend indicates an increase in demand for distributed generation facilities (mostly based on renewable energy sources) and the need for science, market and technology to respond to this demand on time.

It is important to note that the development of distributed generation is associated not only with the use of renewable sources but also with the development of power plants that convert energy to generate electricity and heat.

Today's commercial and residential sectors face three main challenges in the energy sector: electricity costs, supply reliability, load specificity and the release of pollutants to the environment to generate the energy required. A partial solution to these problems will be a distributed energy generation network consisting of local small sources of energy generation.

The cost of energy includes not only the cost of equipment and its amortization costs (CAPEX) but also the payment of the staff for the maintenance of plants, for waste disposal and fuel combustion installations - the logistics costs of fuel transportation and the fuel

payments (OPEX). Distributed systems are spread across the territory, including facilities that are fuel sources, which on average can reduce the distance of fuel transportation and consequently logistics costs. In addition, distributed generation facilities are often plants on renewable energy sources, which often eliminates fuel costs and solve the problem of emissions of pollutants into the environment or reduces it.

Distributed systems are more fail-safe systems because each plant is designed to be used autonomously. By connecting many such plants into a single network, we duplicate each machine with dozens of others, thus, when one or several power plants malfunction, consumers will not be left without access to electric energy. Such systems will be most relevant in private residences with autonomous personal power supplies.

One of the promising types of low-power plants for decentralized power supply systems are high-speed microturbine power plants based on gas or steam turbines, in the latter case operating on organic Rankine cycles. Such plants can use either natural or biogas as fuel (gas turbines) or solid biofuel and waste for combustion in waste heat boilers to supply heat to the working fluid of the cycle. The use of low-boiling-temperature working fluids in the Rankine cycle makes it possible to use plants for the utilization of waste heat from powerful diesel generators of locomotives, industrial processes such as the production of steel or glass.

1.2 Place of application and tasks set for low-power turbogenerators

Low-power turbine generators can act as autonomous units in generating electric and thermal energy both for a distributed network or for personal needs.

Gas microturbines allow the generation of electrical energy for many classic needs, such as supplying electricity to industrial and private consumers. The main disadvantage of such plants is the explicit binding of the plant to the gas access point.

During the construction of distributed energy facilities, we often deal with settlements and facilities located at a distance from centralized energy and gas transmission systems. For example, more than 20 million people live in such regions in different parts of Russia. Imported fuel sharply increases the cost of a unit of produced heat and electricity. The use of microturbine installations operating on local renewable fuels makes it possible to effectively solve the problem of energy supply for such regions, settlements, industrial and other facilities.

The use of local fuel or waste, possibly with a low calorific value, can be effectively carried out by replacing steam in the Rankine cycle with an organic working fluid with a low

boiling point. That allows to have a low temperature of the heat supply source in the thermodynamic cycle. These plants can be used to supply power to remote objects by recycling pellet fuel or wood, supplying electricity and heat to several private houses. Due to the high rotation speed of the microturbine the power plant can be made compact, which will allow it to be used as a transportable energy source.

The use of an organic working fluid opens possibilities for the utilization of waste heat. Instead of a waste heat boiler, there should be a heat exchanger that transfers heat to the working fluid. Such units are used as recuperative units in the thermal cycles of production processes using heat to its fullest extent and reducing thermal pollution of the environment. Such plants are completely dependent on the main production process and do not harm the environment. An example of the use of such plants can be their use at the tail of a diesel generator of a locomotive, where the temperature of the exhaust gases at the outlet is about 300° C. In addition, an example can be production of steel, when the metal is heated, a huge amount of heat is emitted to the environment. Waste heat can be useful for energy conversion.

Due to the high rotational speed and the power electronics unit for the formation of the necessary parameters of electricity, the power plant itself has relatively small dimensions and can be used both as a power plant and in places of special purpose. For example, as an auxiliary air generating unit on an aircraft, where the weight and dimensions of the machine play a significant role or hybrid vehicles.

Due to the huge areas of application of classical high-speed microturbine low-power plants on variations of the Rankine cycle, further emphasis in the work will be dedicated on this type of plant.

1.3 A brief overview of manufactures of low-power turbogenerators

Mankind always needs electricity and heat. Therefore, the energy sector is the most profitable in the industry. Considering small-scale energy and low-power turbine units, it is also necessary to consider the most typical solutions of manufacturing companies to fill the market needs for such units. Article [4] examines the general situation in the world market for ORC technologies. Below we will consider examples of companies and their model ranges of equipment and some characteristic properties.

One of the most well-known manufacturers of microturbine units is Capstone Turbine Corporation. Capstone manufactures gas microturbines the designs of which from type to type in the line do not undergo significant changes with each other. The company has several

versions of machines with nominal capacities: 30 kW, 65 kW, 200 kW, 600 kW, 1 MW with electrical efficiency of 26 %, 29 %, 33 %, 33 %, 33 %, respectively. The plant can use natural gas, kerosene, aviation fuel, biogas, etc. Capstone is one of the few companies to use foil gas-dynamic bearings in their devices.

EXERGY specializes in the production of equipment for the implementation of the organic Rankine cycle and power generation. The unit capacity of this company's equipment ranges from 1 to 20 MW of electricity. The maximum claimed efficiency of the thermodynamic cycle is 30 %. The company provides solutions for the use of biomass, geothermal energy sources, and the use of waste heat from thermal power plants and industrial processes. A characteristic feature of the company is the use of radial turbines.

One of the largest companies in the development of ORC plants related to small plants is Turboden, part of the Mitsubishi Heavy Industries group of companies. Turboden provides equipment ranges from 200 kW to 20 MW. The company provides its own solutions in the areas of biofuels, geothermal energy, waste heat and solar energy. Thermal oil is used as a buffer for transferring thermal energy from the heat source to the working fluid of the plant. The claimed efficiency of the equipment to generate the electrical energy is in the range of 17-24 %. The minimum temperature at the turbine inlet is 240 degrees Celsius. Well-proven axial-flow turbines are used as turbines in power plants.

Siemens and Turboden recently launched a joint line called Heat ReCycle solutions. The equipment is a power plant equipped with Siemens gas turbines ranging from 10 to 68 MW (SGT 300 - 750 series) and ORC-installed systems from Turboden. Thermal oil or cyclopentane is used as a fluid for transferring heat from the exhaust of gas turbines to the system on an organic working fluid. In the system, the companies managed to achieve a high plant efficiency of about 47-50 %, low emissions of pollutants into the environment, and a power generation system that does not use water at all.

ElectraTherm, part of the Bitzer Group, has a rather unusual solution for waste heat recovery concerning the market. The company manufactures equipment for the utilization of low-grade heat with a temperature of 70 to 150 degrees Celsius to generate 75-125 kW of electricity. A screw expander with a working fluid R245fa is used as the converter of thermal energy into mechanical energy. The system needs cooling water with a temperature tolerance of 4 to 65 degrees Celsius.

Clean Energy Technologies (CETY) provides its solution for efficient use of waste heat. CETY provides modular equipment for generating 50-140 kW of electrical power, which uses a radial-axial turbine with a rotational speed of 27 500 rpm, based on magnetic bearing

technology. Equipment to deliver heat to the working fluid (R245fa) uses thermal oil or hot water.

Triogen has two branches of equipment on the ORC cycle. Triogen relies on technology developed originally at LUT. The first is the use of waste heat from gas and diesel engines, the second is the use of heat from the combustion of biofuels. The required flue gas temperature is 350 degrees Celsius, the useful electrical power of the units is in the range of 92 to 162 kW, and the electrical efficiency is in the range from 14.6 % to 17.2 %. The main heat sources for the equipment are flue gases, combustion products or hot air, and water or a mixture of water and glycol is used for cooling in the condenser. A radial single-stage turbine with a rotational speed of 18 000-28 000 rpm is used as a propulsion engine for the generator, the working fluid is toluene, and sleeve bearings lubricated by the working fluid are used.

The Spanish company RANK manufactures a wide range of equipment generation of heat and power. The Rank micro line has a minimum installed power of the equipment up to 2.5 kW at an inlet temperature of 90-120 degrees Celsius. The company also has lines LT 1-3, MT 1-3, HT 1-3, HTC 1-3. Letter designations are responsible for the temperature at the entrance to the equipment (from 90 to 210 degrees Celsius), and the numbers for the serial number in the temperature group by power (minimum LT1 8-20 kW, maximum HTC3 100-145 kW electrical power).

According to the given trend in [4], the microgeneration market based on ORC cycles has been a fast-growing market in the last 20 years. Most of the installed capacity comes from geothermal energy sources, and most of the installed plants are operated for the beneficial use of waste heat.

From the provided information it could be concluded that the company's proposals currently cover all possible areas of application of mini-CHP plants, but at an average power for private use, and as can be seen, the initial power range of the manufacture lines starts from ~ 50 kW, which is a little bit excessive.

1.4 The main components of the machine

A turbogenerator usually consists of three main parts: a turbine, an electric generator, a power electronics unit, and the machine control system.

The turbine consists of a nozzle system and an impeller, a control valve and a shut-down valve. The nozzle system is designed to increase the gas flow rate, thereby increasing the kinetic energy of the flow. The nozzle gives the flow a certain angle of attack on the impeller blades. The nozzle system can be made both in the form of blades or channels with a decreasing channel cross-section. The turbine impeller converts gas energy into mechanical energy of the shaft and transfers it to the drive device. The impeller is attached to the turbine shaft, which can be shared for the entire machine, or separately connected to the generator shaft through a coupling. The turbine housing must be sealed against leakage of the working fluid into the environment.

An electric generator is most often a synchronous generator with permanent-magnet excitation for an autonomous start of a power plant. Depending on the rotational speed and power of the machine the rotor of an electric generator can be either a single cylindrical permanent magnet or a prefabricated structure with an assembled structure of permanent magnets glued on it. The rotor of an electric generator, depending on the application and power, can be located on friction bearings, magnetic bearings, gas-dynamic bearings. In the latter case, it is necessary to provide some gas circulation inside the generator stator. In this case, a certain leakage of the working fluid into the generator stator from the turbine is on purpose carried out. In this case, the design of the generator stator must also be sealed and waterproof. To cool the electric generator on its stator part a radiator is applied to remove heat. Working fluid is also blown over the electric generator or an external cooling by using a fan can be used.

A power electronic unit is required to form the needed parameters of electricity for the consumer. Since in most cases the rotor has a non-constant frequency not bound to the 3000 rpm rotation frequency, the voltage frequency at the terminals of the electric generator is significantly different from the 50 Hz required by the consumer. To solve this problem a power electronics unit consisting of a rectifier and a subsequent inverter to create the required voltage and frequency level is used.

1.5 Existing design solutions

Most manufacturers of turbine generators supply a whole range of equipment to ensure the operation of the unit in an already assembled container, similar to a container for sea transportation. Containers are a modular system that can be efficiently and quickly transported and expanded to suit the needs of the consumer.

One of the most popular examples to consider is Capstone C30 unit [5] with a power of 30 kW and an electrical efficiency of 26 %. The consumption of combustion products of natural gas is 0.31 kg/s, and their temperature at the outlet from the exhaust pipe is 275 °C. Output voltage is 400/480 VAC, 50/60 Hz, 3 phase unit.

It contains the classic components of a low power gas turbine unit: a radial-axial compressor, a combustion chamber, a radial-axial gas turbine. The compressor and the gas turbine are located on the same shaft which is supported by gas-dynamic bearings. Air is fed to these supports due to compressor air suction and in more powerful plants additionally by an impeller from the side of the shaft which is free from the compressor. Combustion products after the gas turbine pass through the diffuser, which increases the heat drop on the turbine, and then enter the recuperator located in the turbine housing. The use of a recuperator in the thermal circuit makes it possible to increase the efficiency of the Brayton cycle by heating the air in front of the combustion chamber with exhaust gases.

The unit is supplied in the form of a container weighing 405 kg and has the following dimensions: width 0.76 m, depth 1.52 m, height 1.96 m.

Another interesting design [6] belongs to the EXERGY company. The machine has an axial supply of the working fluid, a radial turbine in which the gas moves from the center to the periphery. The number of turbine stages on one disk can be up to seven. The turbine rotor rotates on sleeve bearings and is connected to an external electric generator using a coupling.

ElectraTherm supplies power plants in the form of containers weighing 3290/4273 kg (4400B / 6500B series) and dimensions: width 2.4 / 2.0 m, depth 2.0 / 3.3 m, height 2.3 / 2.5 m for the 4400B and 6500B series respectively. The plant has an engine - a screw expander, which converts gas energy into mechanical energy. The expander's output shaft transmits mechanical energy to the generator through a belt drive. The nominal voltage values of the generator are in the range of 380-500 V, 3 phases, the voltage frequency is 50/60 Hz, the power factor of the generator ranges from 0.9 to 1.

In brochure [7] presented CETY power module. The power module includes a radial-axial turbine mounted on the same shaft as a generator. The gas stream flows from the

periphery to the center and passes through the waterproof sealed generator cooling it. The rotor is mounted on magnetic bearings, the rotor speed is maintained at 27 600 rpm. The power unit has an output voltage of 400/480 V, 3 phases, frequency 50/60 Hz. The system is delivered in a container with a mass of 3523 kg and dimensions: width 3.6 m, depth 1.22 m, height 2.16 m.

RANK manufactures equipment similarly in supply containers, the minimum mass has a Micro series about 750 kg with a power of 0.5-2 kW, the 3-phase voltage of 400 V and a frequency of 50 Hz. Container dimensions: width 0.8 m, depth 1.2 m, height 1.45 m.

In [8], the authors have developed a turbine generator with a nominal rotation frequency of 26 000 rpm and a rated power of 50 kW. As can be noted from the work, the turbogenerator consists of a radial-axial turbine, which is attached to the generator shaft. The rotor of the machine is mounted on gas-static bearings. The working fluid is fed through a spiral chamber, used working fluid exits along the generator axis. The generator is cooled by circulating cooling water.

The authors of [9] have developed a steam turbine unit. The initial steam temperature is 330 degrees Celsius, the rotational speed is 12 480 rpm and the output electric power is 1000 kW. The cross-section of the machine is shown in Figure 6.

The electrical machine in the presented design is an induction generator with a rated power of 1 MW, with a squirrel cage rotor with 20 copper bars, copper connecting rings and internal cooling channels. The machine rotor and windings are cooled by circulating water. The generator has the number of pole pairs equal to one, the number of stator slots is 18, the air gap is 5 mm, the stator winding is short pitched by 7/9. More detailed parameters of the electric generator can be found in [9]

The rotor is supported by active magnetic bearings and backed up by ball bearings. Radial magnetic bearings are well insulated from water and steam inside the stator, the axial bearing is not insulated.

The turbine is attached directly to the rotor end of the induction generator. It is a double-flow radial turbine, to unload shaft from axial forces, with the movement of steam from the periphery to the center. Steam supply to each side of the turbine impeller is own, 4 steam supplier to each impeller side.

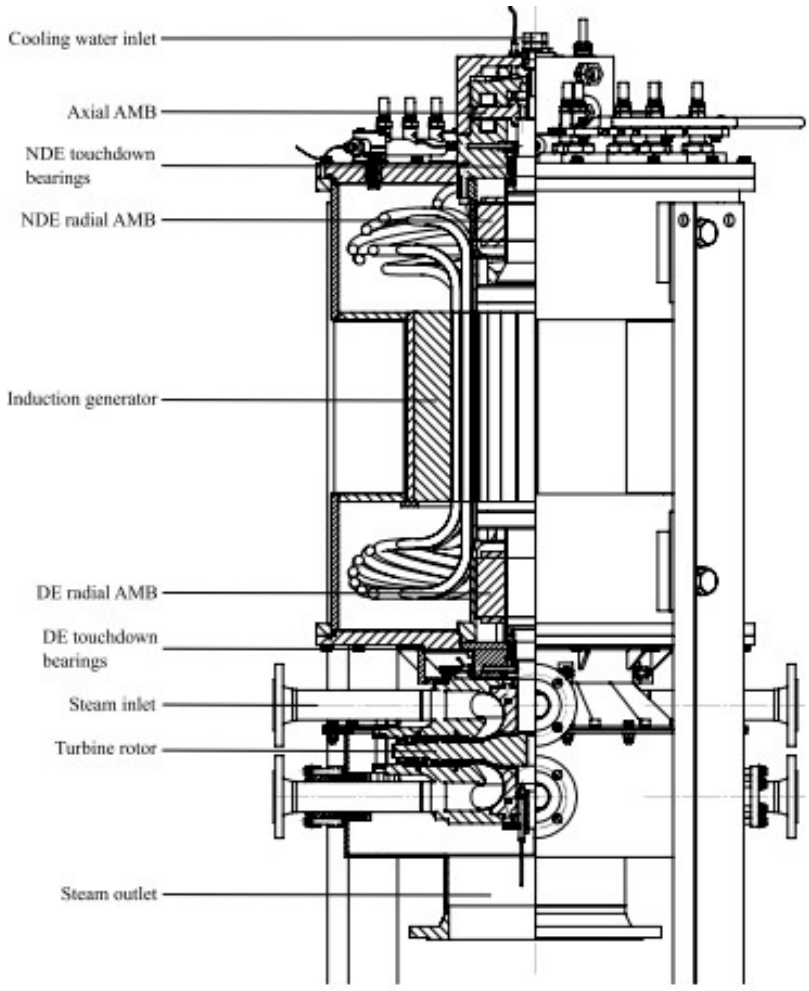

Figure 6: Cross-sectional view of the turbogenerator [9]

1.6 Organic Rankine Cycle: thermodynamic processes

The main idea of the organic Rankine cycle is to replace water vapor with a low-boiling working fluid to be able to use low-temperature heat sources. The main components of the cycle are shown in the schematic diagram in Figure 7.

The primary source of heat is a boiler installation, which burns various types of fuels to transfer the heat flux to the tubes of the evaporator tract. In the tubes of the evaporation tract, the working fluid of the cycle is heated under pressure to the boiling point, evaporates, and, depending on the implementation of the cycle, is superheated to achieve the state of gas without a liquid phase. The process of heat transfer to the working fluid is isobaric and is shown in Figure 7 from point 5 to 0.

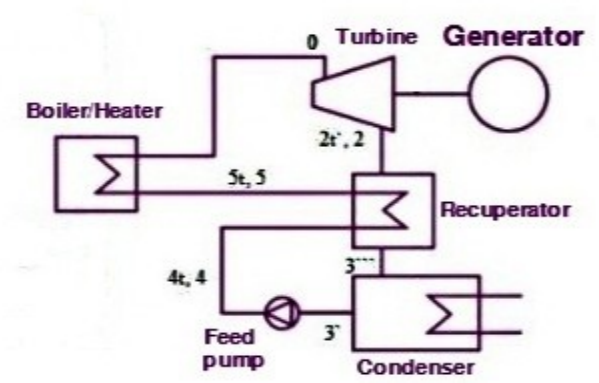

Figure 7: Main components of thermodynamic Rankine cycle

The superheated gas is fed to a turbine, which converts the thermal energy of the gas into mechanical energy of the shaft. If we consider the cycle without taking losses into account, then the process proceeds at constant entropy, points from 0 to 2. The mechanical energy of the shaft is transferred to the shaft of an electric generator to produce electrical energy for consumers.

Exhaust working fluid after leaving the turbine has a low pressure but a high temperature. The high temperature can be effectively used by heating the working fluid before entering the boiler, thereby returning heat to the cycle and significantly increasing the thermodynamic efficiency of the plant. This process is carried out from point 2 to point 3```, by a heat recuperator. It allows using of less fuel to achieve the same temperature heating of the working fluid.

The cooled gaseous working fluid after the recuperator enters the condenser to convert the working fluid from a gaseous state to a liquid. This process is depicted in figure 7 from point 3``` to point 3`. The condenser can be either an air-cooled convector or a heat exchanger supplied with running or circulating water. The largest, but inevitable, heat loss from the cycle occurs in the condenser.

The working fluid in the liquid phase enters the input to the feed pump, which raises the pressure of the working fluid up to the nominal level. The amount of energy required to increase the pressure of the liquid by the pump is several times less than the amount of energy required to increase the pressure of the gas by the compressor. It is the reason why we need a phase transition between liquid and gaseous states. This process takes place from point 3` to 4.

Further, the working fluid under pressure enters the recuperator and is heated by the exhaust gases from the turbine, returning heat to the cycle from point 4 to point 5. At this stage, the cycle is closed, the working fluid moves to the boiler again.

1.7 The problem of choosing a working fluid. Difficulties in conducting experimental studies of plants on the Rankine cycle and conducting experimental studies in air

The tasks of choosing the most successful working fluid for the organic Rankine cycle have already been solved earlier [10, 11], but these works did not consider in sufficient detail the ecological aspects, price, temperature component of the selection of the working fluid, as well as their availability on the market.

Since some working fluids with low boiling temperature fall under the Montreal (about substances that destroy the ozone layer) and the Kyoto Protocols (about greenhouse gases), their use is either limited, and the quota for using them will be reduced year by year, or the use is completely prohibited.

The allowed temperature range of the working fluid is the most important characteristic when the working fluid is applied to the thermal equipment. Organic working fluids have a maximum temperature of chemical stability beyond which, the working fluid begins to decompose into components, losing its physical and thermodynamic properties, and possibly becomes dangerous.

Due to the above facts, various physical and thermodynamic properties, and a massive number of options for working fluids for the cycle, the choice of a suitable working fluid becomes a laborious task.

Also, for further experimental study of the decisions made during the development of a power plant on the organic Rankine cycle, it is necessary to purchase or develop equipment for organizing this cycle, described above. More various resources can be spent on the purchase of equipment or its development than on conducting the actual scientific research on this equipment.

To test high-speed low-power turbine installations, it is proposed to use model tests of a turbogenerator on an air gas-dynamic stand with a variable initial pressure in front of the turbine. This method allows getting rid of a huge amount of equipment costs for organizing the entire Rankine cycle by replacing the working fluid with air, which can be supplied to the turbine generator by a compressor.

This method allows a series of experiments to be carried out on simpler equipment and to extrapolate the result through the semblance of gas-dynamic processes from the air, which is the working fluid in the experimental setup, to low-boiling liquids. Thus, it is possible to

obtain many studies of gas-dynamic processes in a turbine unit before the actual assembly of the power plant at an ORC.

Two gas flows will be similar if the characteristics of one of them can be obtained by multiplying the characteristics of another flow by constant coefficients. For such a simulation should be observed the geometric similarity of sizes, the similarity of speeds, and the similarity of forces. In more detail, to model a stationary flow, it is necessary to observe the geometric similarity, the similarity of the velocities, and the equality of the Reynolds and Froude numbers (when compressible fluid is taken into account, to this series of values should be added Mach number). If the mass forces do not play a decisive role, then the simulation is carried out at a constant Reynolds number.

2. Gas-dynamic test stand

Testing high-speed devices can be performed in a test stand based on the use of pressurized air. Such a test stand is described below.

2.1 Test stand gas-dynamic path

Performing the calculation stage by finite element methods of equipment prototypes, in general, still requires verification of the results through experimental data. These data can be obtained on equipment models or directly from prototypes during tests on specially designed and equipped stands. As mentioned earlier, the application of the theory of the similarity of gas-dynamic processes makes it possible to extrapolate data from experimental results to a full-scale model even on a different working fluid.

To obtain the characteristics of a high-speed low-power turbogenerator, gas-dynamic test stand, such as described in [12], can be used. The stand appearance is shown in Figure 8 and the installation diagram is shown in Figure 9.

Figure 8. General view of a gas-dynamic test stand

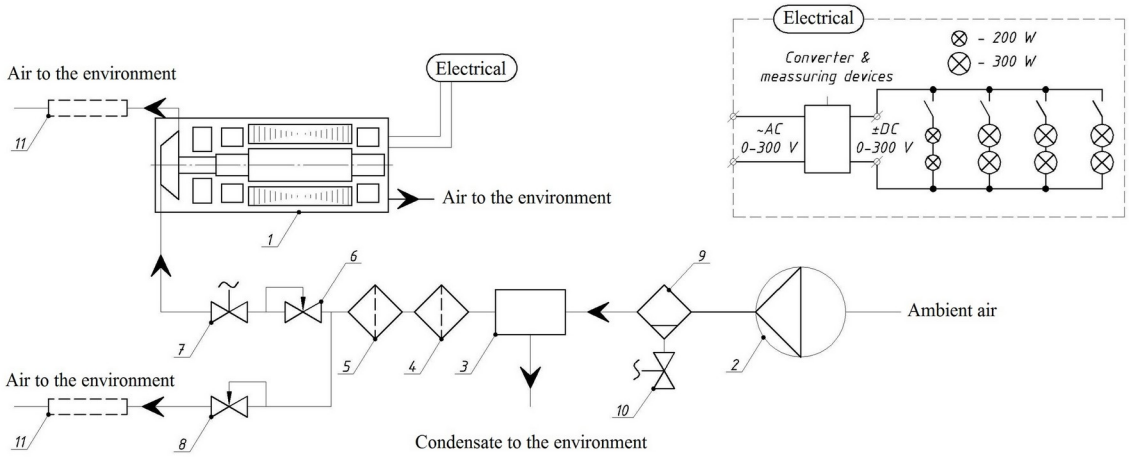

Figure 9. Functional scheme of the gas-dynamic test stand. 1 Device under test, 2 Compressor, 3 Cryogenic air dryer, 4, 5 Air filter, 6 Control valve, 7 Shut-down valve, 8 Dump valve, 9 Liquid phase separator, 10 Condensate drain valve, 11 Silencer.

The nominal parameters of the test stand, shown in Figure 8, are the nominal pressure at the inlet to the turbine unit 0.75 MPa and the volumetric airflow rate under normal conditions 1.48 m^3/min. These characteristics allow to test turbine units with a power of up to 5 kW and a speed of up to 200 000 rpm.

The stand takes air from the environment using a screw, oil-filled compressor shown in Figure 9 under number 2. Compressed air enters the liquid phase separator at number 9, from which condensate is drained through valve 10. The prepared compressed air then going towards a cryogenic dryer, where the air is cooled to the dew point. Lost moisture also is drained into the environment. The dehumidified and cooled air at the outlet of the dehumidifier is heated from the dehumidifier's radiator and passes through of medium filter (number 4) and fine filter (number 5). Usually, a balanced receiver is installed in the same line with the compressor to keep the pressure in the compressor line constant. In this design, the system for maintaining a constant pressure in the line is carried out using a method of two hydraulic regulators with the possibility of manual adjustment. The first regulator “getting feedback from the pressure after itself” is installed in the load line and is shown under number 6. It maintains the pressure in the line constant after itself offering constant pressure at the inlet to the turbine generator. The second “before itself” regulator, shown at number 8, maintains the pressure in the compressor line constant to ensure its normal operation by releasing excess pressure to the environment. Silencers 11 are installed in both lines at the ends to reduce noise during air discharge. A shut-off valve 7 is also installed in the load line, which is part of the protection system against an excessive increase in the rotor speed of the machine.

2.2 Electrical part of the stand and measurement system

The electrical load is simulated by 200 W and 300 W incandescent lamps, which are connected in various combinations to change the load on the generator during the experiment. Since the generator produces a three-phase high-frequency voltage, this voltage must be converted by a rectifier to connect to the load. To simulate a more powerful load, there is a resistive ballast connected instead of lamps as a consumer.

To estimate the performance of the tested machine, many measuring devices are installed on the stand. To control the efficiency of the turbine flow path and monitor the stand characteristics, five pressure sensors with 4-20 mA current outputs were installed, where one of them has a measurement range from 0 to 2.5 MPa, the rest from 0 to 1 MPa. Also, there are two spring manometers installed, one of which duplicates the results of the electric pressure sensor. To measure the flow rate through the machine, a diaphragm is installed to measure the pressure difference (from 0 to 4 kPa) on the diaphragm and, accordingly, a sensor with a current output of 4-20 mA. Three thermistors are installed in the load line to measure the temperature. A massive set of possible combinations of parameters can be measured using installed sensors. It allows for a sufficiently detailed study of the gas-dynamic processes in equipment.

All signals from the sensors described above are fed to a microprocessor-based programmable device TPM148 of the OWEN company. It allows to filter signals, perform mathematical calculations, control parameters using the built-in PID controller, and transmit data through the RS-485 interface. In addition to this, a LeCroy oscilloscope is installed to measure voltage and current levels and display waveforms. The presence of a device for measuring electrical parameters makes it possible to test not only electric generators under load but also other electromechanical devices.

All information from sensors is transmitted through interfaces to a personal computer in real-time and stored in databases. It is also possible to connect a LabView program for processing the data of the implementation of an elementary control system for the experiment process.

2.3 Experimental characteristic of the stand

To develop prototypes, it is necessary to obtain not only the quantitative characteristics of individual parts of the equipment but also the parameters of the entire system. To design a turbogenerator, it is necessary to know the actual flow rate and the pressure in the compressor at this flow rate since the pressure determines, in this case, the upper energy limit of the working fluid. In turn, the mass flow rate determines how much of the working fluid passes through the turbine generator in one second.

On the other hand, since the turbogenerator is installed immediately after the shut-off valve, there is an additional hydraulic resistance of the network which the gas has to overcome when moving from machine to the environment. The outlet pressure after the machine will be greater than the ambient pressure, and in case of the increase in this pressure will reduce the energy drop for the turbine. Knowledge of the characteristics of the flow rate and resistance of the network is a necessary foundation for further calculation of the turbine unit.

To obtain these dependencies an experiment on an existing test stand was carried out. Two different pressures inside the compressor, close to the nominal, 6.5 and 7 bar were used. The parameters in the system were changed by varying the settings of the regulators. Regulator 6 was used to change the pressure in the load network, regulator 8 to keep the pressure in the compressor constant and prevent the safety valve from opening. The obtained characteristic of the pressure P_0 after the shut-down valve versus the flow rate in the load line is shown in Figure 10. Figure 11 shows a plot of the dimensionless pressure loss coefficient for the section of the hydraulic network from the shut-off valve to the atmosphere. This loss factor should be taken into account when designing a low-power air turbine unit to take into account the pressure rise behind the pipe relative to atmospheric pressure.

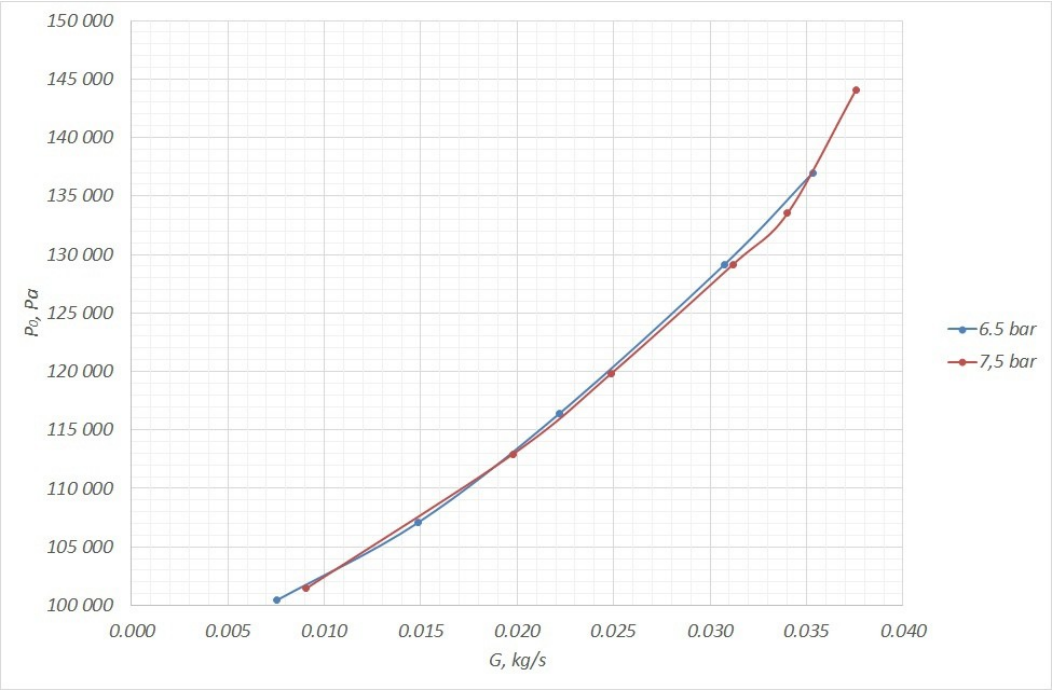

Figure 10: Network characteristics. p_0 represents the pressure right after the control valve 6, i.e. absolute pressure drop in the system.

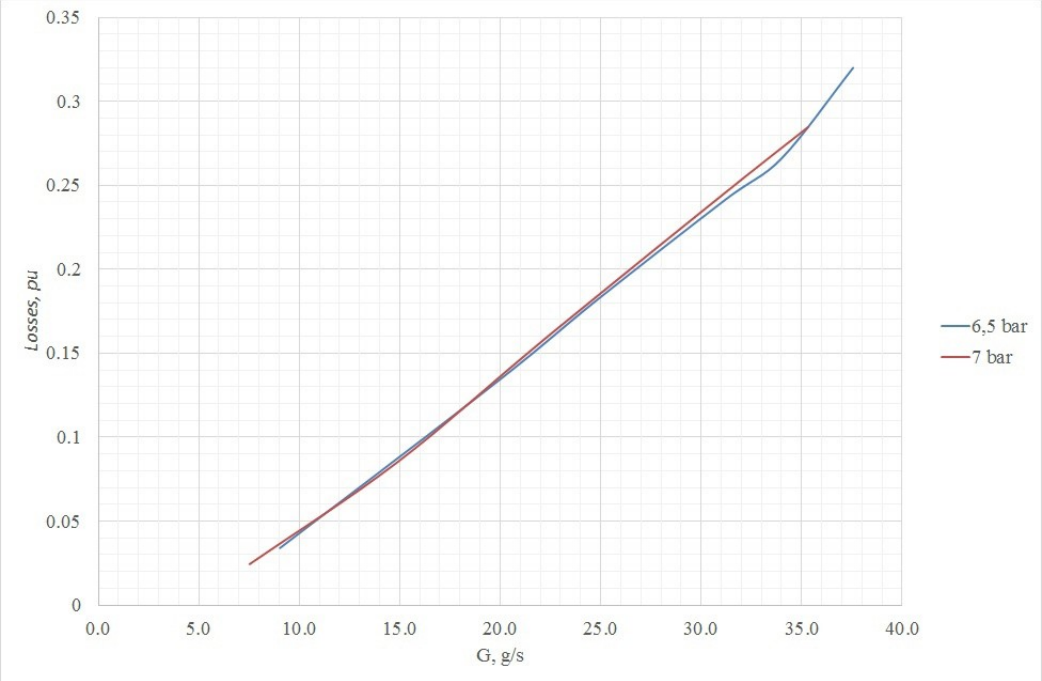

Figure 11: Network loss coefficient

2.4 Turbogenerator design problem

Based on the information received about the test stand, it is possible to set the task of developing a high-speed low-power turbine unit with an experimental rotational speed of 150 000 rpm for an initial pressure in front of the turbine of up to 7 bar, an initial temperature of 29 degrees of Celsius (Average temperature of dry air during the experiment, deviations from the average varied within ± 2 degrees of Celsius). It is necessary to determine the type of turbine and its power with a blade height of at least 4 mm. After completing the design of the turbine, calculate the synchronous generator with excitation from a permanent magnet of cylindrical shape with the number of phases $m = 3$, the number of pole pairs $p = 1$, as well as the voltage in the DC bus 620 V for the possibility of the inverter forming a 220 V phase and 380 V line-to-line voltage.

3. Design process

3.1 Choosing turbine type

When starting to design a machine, it is necessary to determine the type of projected impeller: axial, radial-axial or centripetal. For an initial assessment, we can use the specific-speed formula [13] adapted for turbines:

$$n_s = 11.3 \cdot \frac{n \cdot \sqrt{Q}}{\sqrt[4]{\left(\frac{p_{diff}}{\rho \cdot g}\right)^3}} \tag{1}$$

Where: n_s – Specific speed,

n – Rotation speed in rpm,

Q – Volume flow rate in m^3/s,

p_{diff} – Pressure difference in Pa,

ρ – Gas density in kg/m^3,

g – Gravitational constant.

For the previously established rotation speed of the turbogenerator and network characteristic it is possible to obtain plots of the dependencies of the specific speed on the mass flow rate and pressure drop across the turbine. The plots are shown in Figures 12 and 13.

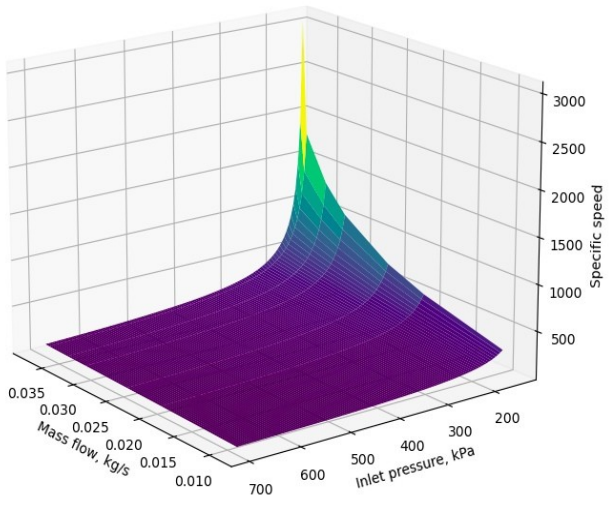

Figure 12: 3D plot of the specific speed

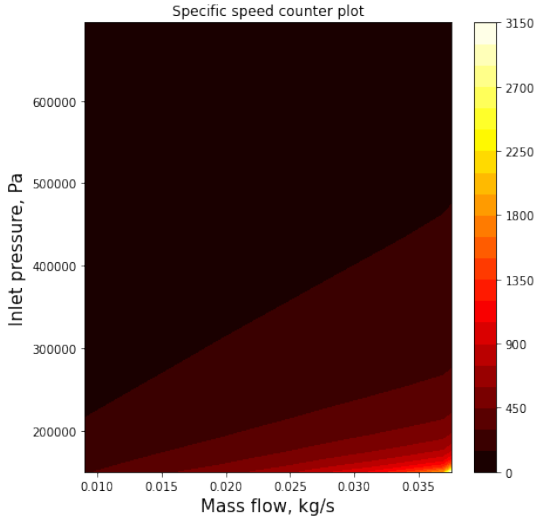

Figure 13: Counter plot of the specific speed

Figures 12 and 13 show that most of the possible specific speeds vary between 19 and 400. The average value of the specific-speed on a surface is 200. This value can be a marker to classify a potential turbine as a low-speed machine, which is often designed in a radial-axial or centripetal type. Usually specific speed from 0 to 150 is suitable for a radial impeller.

Specific speed values from 150 to 400 suit to radial-axial type and values beyond 400 and higher refer to an axial turbine. To prevent the closing of the boundary layers of the liquid, it is necessary to optimize the minimum cross-section between blades which is usually performed by varying blade height. Cross-section optimization usually refers to increasing the blade height to increase the effective cross-section [14]. To increase the height of the blade and to keep a pressure, a speed in a channel the same, it is necessary to increase the mass flow rate [14]. For this reason it is necessary to use the maximum compressor mass flow at the inlet pressure 2.6 bar selected in Appendix 1. With these parameters the specific-speed is 312 referring to radial-axial type of construction.

The axial type of the impeller, in this case, is problematic due to the high speed and low mass flow, which lead to the tiny impeller [14], under constant average diameter, without the possibility of safety fixing it to the generator rotor. Also, the impeller will certainly have blades with a large space between them on the periphery diameter, which will increase the losses of the impeller. Large space between blades on the periphery diameter creates aerodynamically inefficient cross-sections. Usually for axial stage ratio of the average diameter to the blade height should exceed 2.5 [14].

A centripetal turbine was found suitable for the flow and pressure parameters. The height of blades could be more than 4 mm, but the strength calculation of the cantilevered blades showed their unreliability at the rated speed 150 000 rpm. Centrifugal forces create great stress at the root of the blades at the established disk diameter 26.5 mm.

The most rational version is a radial-axial turbine with an inlet of the working fluid tangentially to the rotational axis and an axial outlet from the impeller. This type of turbine is commonly used as a reliable device for low-power plants. This confirms the fact that in the design overview this type of turbine is found most often for low-power turbine units.

3.2 **Turbine nozzle ring**

For a radial-axial turbine, there are at least three different types of nozzle systems: Nozzle system constructed by blades, channel guide system or channel guide system formed by arcs. The approximate estimated angle of the flow exit from the nozzle apparatus is about 10 °.

The nozzle apparatus constructed by blades represent the aerodynamic profiles of the nozzle blades mounted in a circle on a stator around the rotating impeller. The blade shapes have specially designed profiles to create a confusor flow between blades with a given

function of changing the cross-sectional area. In practice, such apparatus can be used on equipment at relatively high powers and flow rates of the working fluid. The reason for the rare use of such nozzle system is that a narrow cross-section at low flow rates of the working fluid becomes impossible to produce with standard milling cutters. In addition, the edges of the nozzle blades are too thin, which leads to their rapid wear or breakage [14]. Such problems lead to a change in the flow aerodynamics in the flow path and a decreasing the efficiency of the equipment. On the other hand, edges could not be too thick because they will create an inefficient aerodynamic profile of blades. To determine the effective edge thickness it is needed to implement some mechanical calculation to find the minimum accepted thickness from a safety factor point of view.

Channel guide system formed by parallel straight lines is an attempt to expand the confuser flow of the working fluid in space. The change in the cross-sectional area occurs not in the impeller rotation plane but perpendicular to it. An example of such a nozzle system is illustrated in Figure 14. Such a guide system allows effective adjustment of the channel height when designing the machine but is practically not suitable for sharper entry angles less than ~15 °. At small angles and diameters, it becomes impossible to place the channels around the nozzle system circle, since collision of the channels would happens. Since the initial assessment estimated (Appendix 1) the outer impeller diameter at 25-30 mm and the flow exit angle from the nozzle system 10 °, some sketches of the nozzle system were created and practically none of them was successful.

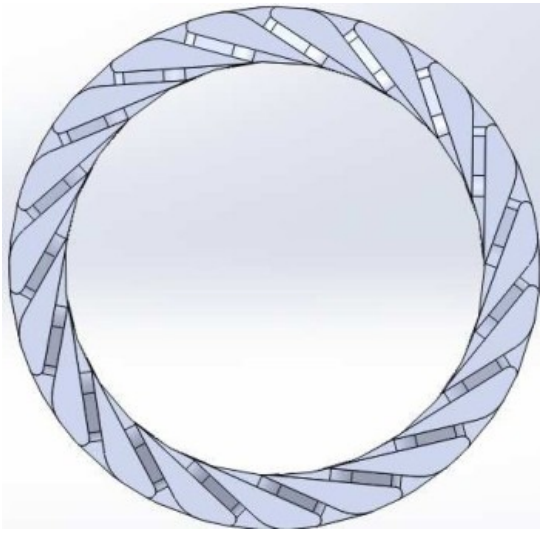

Figure 14: Channel guide system

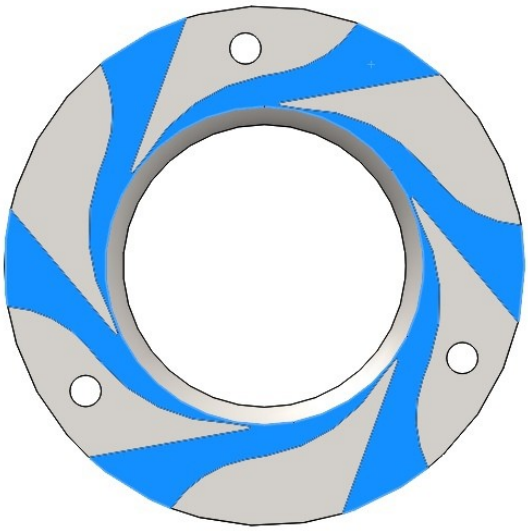

Figure 15: Channel guide system formed by arcs. Gray parts is a steel.

The channel guide vane formed by circular arcs is often used in cryogenic turboexpanders at low flow rates of the working fluid (Figure 15). Such a guide vane is

designed with a small number of nozzle channels for small flow exit angles [15]. Because the throat of the channel is at a sufficient distance from the impeller, some unevenness of the flow angle at the exit appears. Nevertheless, for the inner diameter of the nozzle ring between 25 and 30 mm, this option is practically the only one and it is the best in terms of manufacturing technology.

3.3 Calculations of the flow path

The design calculation was carried out by an iterative selection of the optimal input pressure and mass flow of the working fluid to create an appropriate flow in the channels of the flow path. Calculations carried out based on methods in [14, 15, 16]. An initial pressure of 2.6 bar and a flow rate of 37 g/s were chosen (Appendix 1). One of the main parameters which affect efficiency of the machine is v_d/C_f ratio. v_d/C_f is a ratio of a peripheral speed at the average impeller diameter to a maximum flow speed from the nozzle system to an environment. The calculation of the flow path was carried out under obtained optimal parameter v_d/C_f (Appendix 1), which provides the exit angle from the impeller at 90 °. Thus, the gas energy becomes fully used on the impeller.

The calculation is presented in Appendix 1. Table 1 summarizes the parameters of the working fluid along the gas-dynamic path. Based on its results, a subsonic radial-axial turbine was obtained with a degree of reaction of 0.52 (degree of reaction is ratio of isentropic enthalpy drop in rotor to the total isentropic enthalpy drop in stage [14]) and an outer impeller diameter of 25.5 mm. The height of the impeller blade at the inlet is 5 mm, and the height of the nozzle channel is 4.8 mm. The estimated internal efficiency of the turbine was 81.5 % and the internal power was 1.45 kW. It should be noted that the obtained parameters of efficiency and power will be refined later by FEM calculation, and the current calculation should be considered as an initial approximation.

Table 1. Parameters of air flow in the flow path.

Pressure, kPa	Temperature, K	Specific volume, m^3/kg	Enthalpy, kJ/kg
Parameters before nozzle system			
261	302	0.332	304
Actual parameters behind nozzle system			
198	282	0.408	283
Actual parameters behind impeller			
143	270	0.542	271

3.4 Simulation of the flow path in the turbine using FEM

Based on the calculated values of the turbine 3D model of the flow path was designed and finite element analyses in Ansys CFX performed.

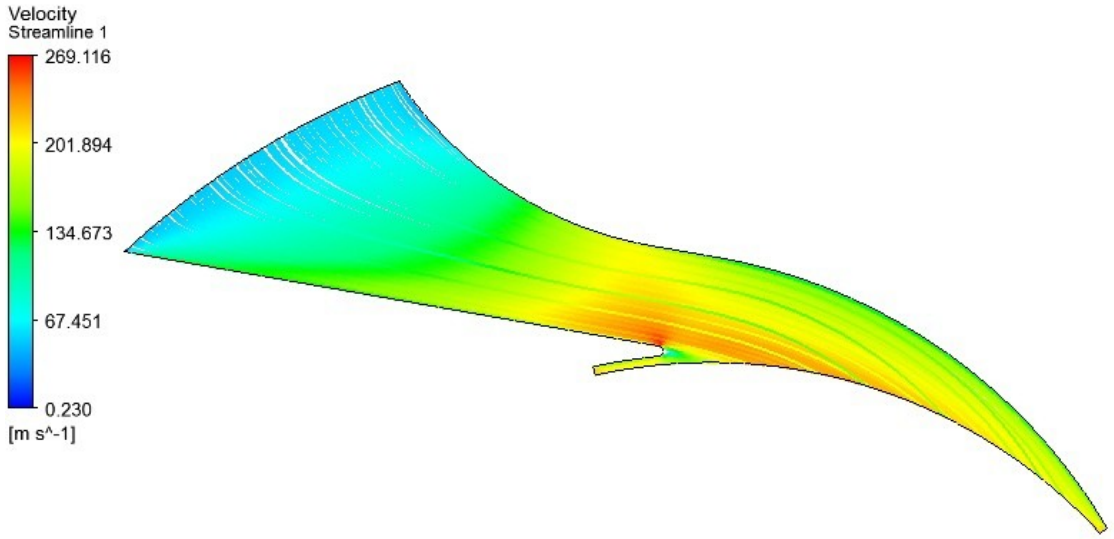

Figure 16: Flow in a channel of the nozzle system

Figure 16 shows the flow of the working fluid in the nozzle system channels. Here only 1/6 part of the nozzle system is shown and simulated. As it can be seen, the model was imposed on the boundary conditions of symmetry and the total air pressure at the inlet to the channel, as well as the static pressure after acceleration of the flow. The resulting flow is strictly accelerated; there are no flow separation from the channel walls.

Further, after the development of the nozzle system, a gas-dynamic calculation of the whole flow path of the turbine was carried out. The impeller was created according to design parameters (Appendix 1) and optimized based on the results of the flow simulation. As a result of the optimization of the flow in the flow path, it was necessary to increase the initial pressure in front of the turbine to 2.8 bar. This was done to reach the rated mass flow, because with the lower pressure the mass flow was lower due a fluid boundary layers. The boundary conditions for the flow path were the total pressure and temperature of the working fluid at the inlet to the nozzle system (A arrow in Figure 17), as well as the static pressure after the turbine (B arrow in Figure 17), which is equal to the calculated one previously in Appendix 1. All other surfaces in model are the walls. The distribution of velocity and pressure along the flow path are shown in Figures 17 and 18. The velocity in Figure 17 is shown for the nozzle and exhaust part in absolute coordinate system, for the impeller the velocity is shown in

relative coordinate system, fixed to the rotating impeller. The angle of exit of the flow from the impeller in absolute motion is 90 degrees, which indicates the correct design of the flow path for the calculated v_d/C_f.

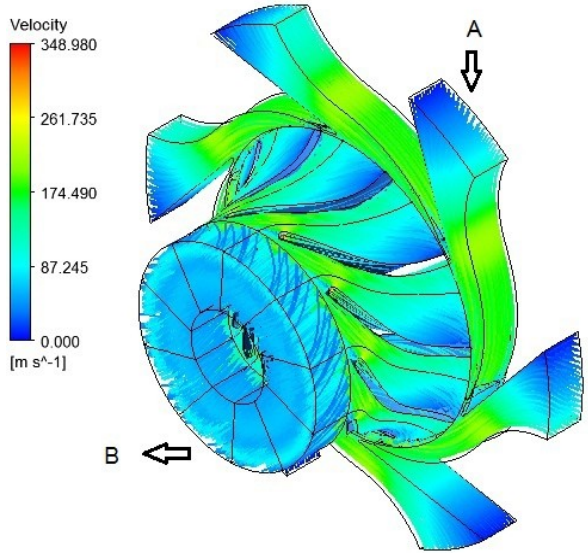

Figure 17: Speed distribution in the flow path

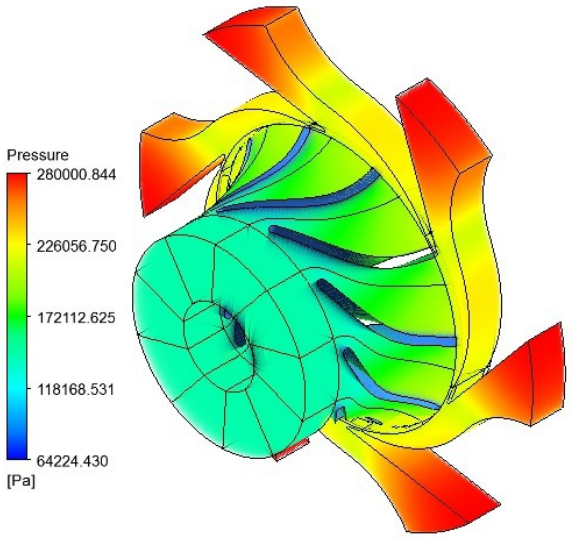

Figure 18: Pressure distribution in the flow path

Figure 19 shows the distribution of the speed in the middle section between the impeller blades. The flow is strictly accelerating without separations and backflows. The flow in the impeller is good, as expected.

The obtained numerical results from simulations clarify the parameters of the flow, power, and efficiency of the flow path received from the previous stage. The initial pressure should be 2.8 bar, the internal power of the turbine is 1.7 kW, and the internal efficiency is 86.2 %.

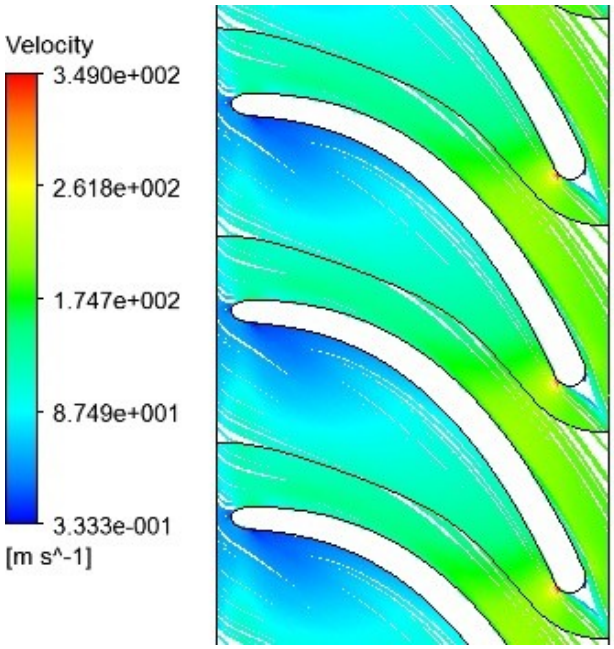

Figure 19: Blade-to-blade speed distribution on average diameter

3.5 Strength calculation of the impeller using FEM

The resulting geometric representation of the turbine impeller is shown in Figure 20. The manufacture of this impeller was planned by casting from aluminum alloy 6061 T6. The material 0.2 % offset yield strength is 280 MPa, and the density is 2770 kg/m^3. To consider the stress of the impeller, it is sufficient to consider the stress of its blades. The maximum stress is expected to take place at the root of the blade under maximum blade height.

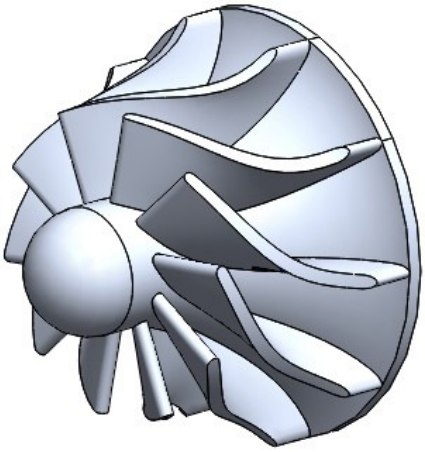

Figure 20: Impeller's appearance

The boundary conditions for the simulation in Ansys Mechanics are presented in Figure 21. Letter A shows the boundary condition for the rotation of the rotor blade around the axis of the impeller at a speed of 150 000 rpm. Letter B denotes a plane of rigid support which imitates the inseparable connection of the blade with the impeller's body. Letter C denotes the pressure distribution over the blade surface taken from the previous step in the simulation of the flow path. Here is the same pressure as is shown in Figure 18 acting on the blade.

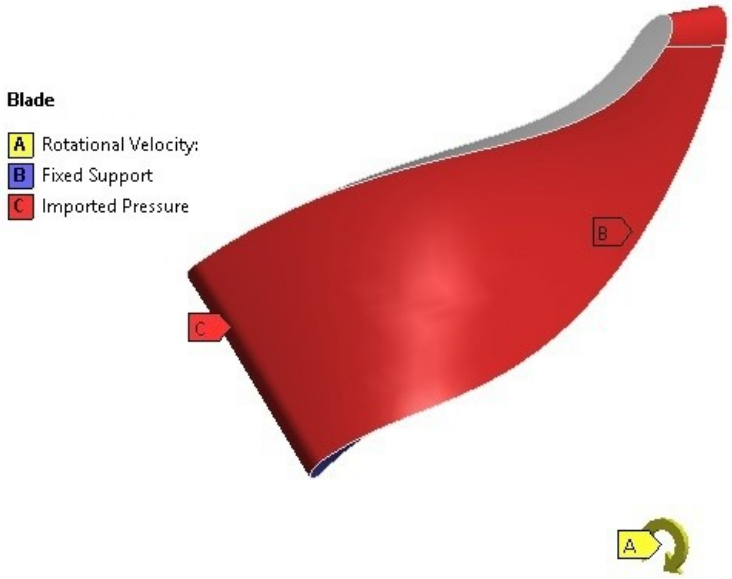

Figure 21: Blade boundary conditions

As a result of the calculation, the distribution of stresses (Figure 22) and the safety factor (Figure 23) over the blade surface were obtained. It should be noted that the highest stress of 120 MPa occurred at the expected point, stress does not exceed the yield stress of the material. The minimum safety factor was 2.3, which allows the blade to perceive stochastic dynamic loads during operation.

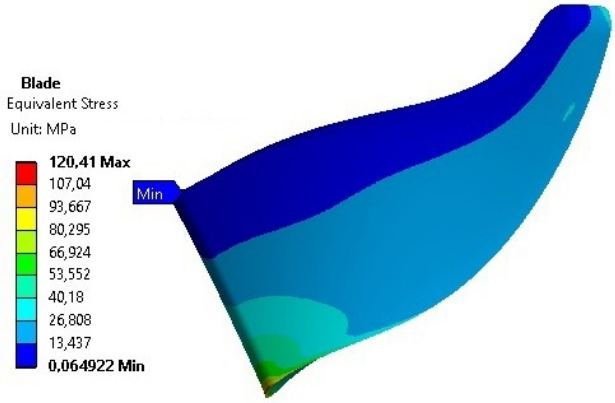

Figure 22: Stress distribution for the blade

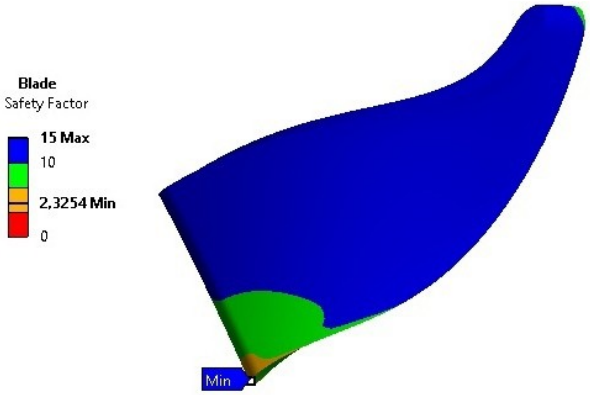

Figure 23: Safety factor distribution for the blade

3.6 Choosing permanent magnets

An important task for the engineer during the design process of an electrical generator is the selection of active rotor materials because this will subsequently lead to impacts on the generator design. The materials for the magnet can be Al-Ni-Co-Fe, Fe-Cr-Co, Nd-Fe-B or SmCo.

Al-Ni-Co-Fe can be used in manufacturing permanent magnets by casting. It distinguishes itself in tensile strength of the order of 30-40 MPa and stability at temperatures up to 550 degrees Celsius but has a low energy product BH_{max} (60-70 kJ/m^3) relative to the levels of modern magnets, as well as a steeply falling demagnetization curve. Its remanence is high but coercive force very low [17].

Fe-Cr-Co alloy is also a material for making permanent magnets. Let us take the material 25X15KA for a specific example. The alloy has 686 MPa yield strength [18], an operating temperature of 400-450 degrees Celsius, as well as a similarly low energy product BH_{max} (32-36 kJ/m^3), and a steeply falling demagnetization curve [19].

Nb-Fe-B is the most common and readily available permanent magnet material for high-speed turbomachines. Neodymium magnets have an energy product BH_{max} of at least 150 kJ/m^3, the tensile strength of the order of 70-130 MPa [20], low corrosion and radiation

resistance, and operating temperature (up to 180 degrees Celsius) [21, 22]. The demagnetization curve of this material looks like a monotonically decreasing linear function which is a desirable property.

Rare earth permanent magnets based on SmCo alloy have almost the same high energy product as neodymium magnets and a similar demagnetization curve, but they have high-temperature stability (up to 250 degrees Celsius and higher), the value of the temperature coefficient of flux density (B_r) is -0.035 %/°C, in contrast to -0.11 %/°C for magnets based on Nd-Fe-B, and also has a high radiation resistance, which makes magnets indispensable in aviation and rocketry [23]. The tensile strength is 35-40 MPa [24, 25].

Although the developed air turbogenerator is an experimental model for testing on a gas-dynamic stand, the main application of machines of this type is working as part of organic Rankine cycle, in which the defining parameters for choosing a magnet can be: high energy product, the ability of the magnet to operate at temperatures hundreds of degrees higher than the ambient temperature, and also high corrosion resistance. Based on these facts, the most suitable material for a permanent magnet rotor is a magnet, based on the rare earth alloy SmCo.

3.7 Strength of the magnet-sleeve system

As noted earlier, a magnet based on the rare earth SmCo alloy has a tensile strength of about 35-40 MPa. This value is very low for simple use of a permanent magnet as a shaft. To prevent destruction of the rotor at high speeds and, as a result, high centrifugal forces, a strong steel band is installed on the magnet with hot interference. In our case, we will use 36НХТЮ precision spring steel (non-magnetic steel with 785 MPa yield strength with shares of nickel, chrome, titan, and aluminum [26]).

Since the rotor body is a fragile permanent magnet that does not work in tension, it is reasonable to arrange stresses in the center of the magnet equal to zero or some small negative number. Since the magnet without a band operates in tension from centrifugal forces, the greatest stresses will be in the center. To calculate the stresses in a magnet, we will use formula for radial stresses, since in the center of rotation of each cylindrical object without holes the radial and circumferential stresses are equal to each other. The resulting stress will be the stress that the band must apply to the rotor so that at the rated speed in the magnet the stress is equal to the predetermined number.

$$\sigma_r(r) = \sigma_{(r\ press)} + \frac{3+\nu_{pm}}{8} \cdot \rho_{pm} \cdot \Omega^2 \cdot (r_{pm}^2 - r^2) \quad (2)$$

Where: σ_r – Radial stress in Pa,

$\sigma_{r\ press}$ – Radial stress from shrink fitting (in our case equal zero) in Pa,

ν_{pm} – Poisson's ratio for permanent magnet,

ρ_{pm} – Permanent magnet material density in kg/m^3,

Ω – Rotation speed in rad/s,

r_{pm} – Outer radius of permanent magnet in m.

To obtain a safety factor in the bandage necessary to calculate the stress of the band fitted with an interference fit on a permanent magnet, which at the rated speed will create a pulling force equal to the value obtained by formula (2) at zero radius. The check of the stress must be carried out in two states of the rotor. The first one is at the nominal rotational speed. At this moment, the forces from the interference and centrifugal force act on the band. The second is a state of the rest (zero speed) because the force which acts on the magnet will be greater than at the nominal load.

To understand not only qualitatively but also quantitatively how the diameters of the rotor system change depending on the rotor speed of the turbogenerator and the diameter of the permanent magnet selected when designing (based on some calculations using the methodology outlined above, and in a formulaic form in [27]) a plot was built (Figure 24), illustrating the dependence of bandage thickness on the diameter of the magnet and the rotor speed. Curves ends where safety factor for the sleeve becomes less then 1.2. Figure 25 shows the dependence of the safety factor of the bandage on the diameter of the permanent magnet and the rotor speed.

In calculations, it was assumed here and below that the magnet material used is SmCo5 and the stress at the center of the magnet at the nominal operating mode is 0 MPa. Since for high-speed turbomachines the minimum thickness of the magnet retaining sleeve for small diameters of the magnet, about 5 mm, are not feasible for technological reasons due to the small thickness of the sleeve, we assume that the minimum size of the sleeve thickness is 1 mm. To make the possibility of comparing several variants of pairs the rotational speed - the diameter of the permanent magnet, we take the nominal safety factor equal to two, which we will adjust. In case when safety factor less than 2, we optimize a thickness of the sleeve to reach maximum possible safety factor.

For a given rotor speed of 150 000 rpm, Table 2 summarizes the calculation results.

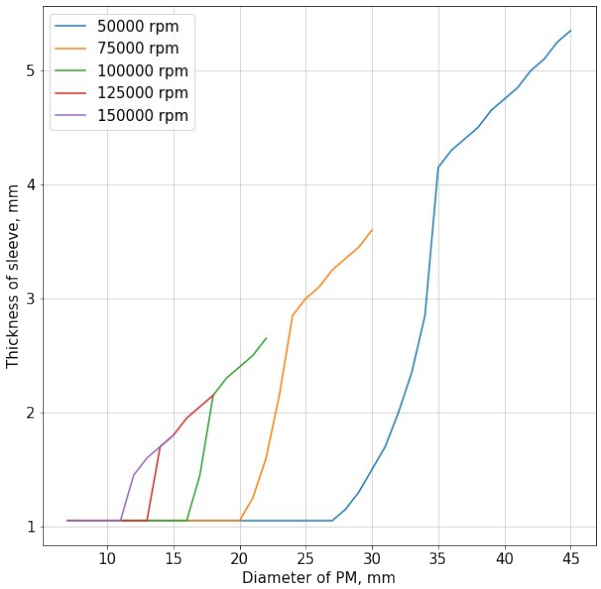

Figure 24: Dependence of magnet retaining sleeve thickness on PM diameter and rotation speed

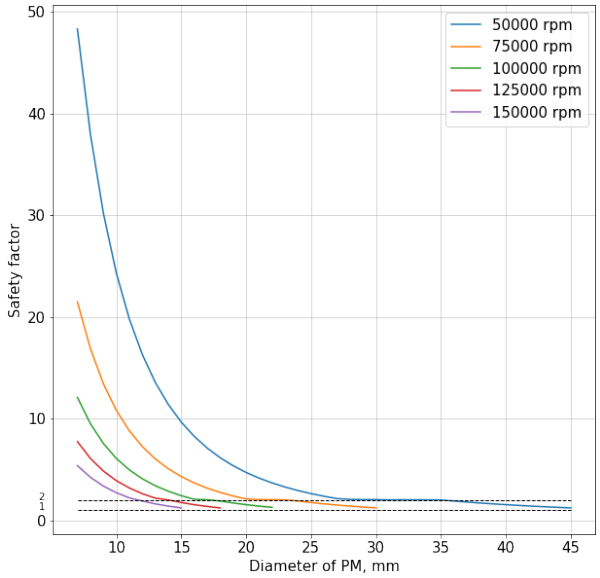

Figure 25: Dependence of safety factor on PM diameter and rotation speed

Table 2. Sleeve thickness, safety factor, interference at rotation speed 150 000 rpm

Permanent magnet diameter	Magnet retaining sleeve external diameter	Magnet retaining sleeve thickness	Safety factor	Shrink fitting
mm	mm	mm	-	μm
6	8	1	7	1.48
7	9	1	5.3	2.45
8	10	1	4.2	3.83
9	11	1	3.3	5.74
10	12	1	2.6	8.30
11	13	1	2.1	11.65
12	15	1.5	1.85	13.29
13	16	1.5	1.6	17.25
14	17.5	1.75	1.38	20.50
15	18.5	1.75	1.2	25.96
16	20.5	2.25	1.04	29.35

3.8 Estimation of the magnetic flux density in the air gap

In the design of electric machines, including electric generators with permanent magnet excitation for high-speed turbine units, it is necessary to set a large number of variables [28]. Among them is the magnetic flux density in the air gap. It is difficult to choose these variables without having experience in designing electrical machines at the manufacturing level. Moreover, for high-speed machines (40-300 krpm), there is practically no sufficient amount of statistical data.

To simplify the process of setting the magnetic flux density, as well as to exclude this parameter from the equation of the main dimensions of the generator, I derive the dependence of the magnetic flux density on the diameter of the permanent magnet.

Let us assume that the magnetic flux density along the radius of the gap behaves linearly according to the formula:

$$\frac{B(x)}{B_{\mathrm{m}}}=\frac{d_{\mathrm{m}}}{d_{\mathrm{m}}+2x} \tag{3}$$

Where: B_{m} – Magnet flux density amplitude close to magnet surface in T,

$B(x)$ – Magnet flux density amplitude at point in the gap in T,

d_{m} – Outer diameter of magnet in m,

x – Coordinate along the radius in the gap in m.

Then formula (3) could be rewritten into the form:

$$B(x)=\frac{d_{\mathrm{m}}}{d_{\mathrm{m}}+2x}\cdot B_{\mathrm{m}} \tag{4}$$

Accordingly, the magnetic field strength in this case:

$$H(x)=\frac{d_{\mathrm{m}}}{d_{\mathrm{m}}+2x}\cdot\frac{B_{\mathrm{m}}}{\mu\cdot\mu_0} \tag{5}$$

Where: μ – relative magnetic permeability of air,

μ_0 – magnetic permeability in vacuum.

The magnetic voltage for the gap can be calculated as follows:

$$F=\int_0^{\delta}H(x)\,\mathrm{d}x=\frac{B_{\mathrm{m}}}{\mu\cdot\mu_0}\int_0^{\delta}\frac{d_{\mathrm{m}}}{d_{\mathrm{m}}+2x}\,\mathrm{d}x=\frac{B_{\mathrm{m}}d_{\mathrm{m}}}{2\mu\cdot\mu_0}\cdot\left(\ln\left(2\delta+d_{\mathrm{m}}\right)-\ln\left(d_{\mathrm{m}}\right)\right)$$
$$F=\frac{B_{\mathrm{m}}d_{\mathrm{m}}}{2\mu\cdot\mu_0}\cdot\ln\left(1+\frac{2\delta}{d_{\mathrm{m}}}\right) \tag{6}$$

Where: δ – Gap length in m.

Since demagnetization occurs from two poles of the magnet, the demagnetizing magnetic voltage is $F_{dem} = 2 \cdot F$, and the demagnetizing magnetic strength is $H_{dem} = F_{dem} / d_m$.

SmCo magnets have a straight line in the hysteresis loop in the second quadrant (Figure 26).

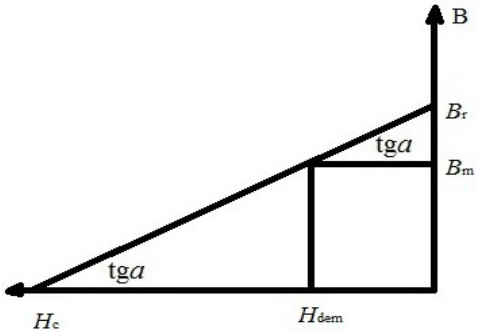

Figure 26: Hysteresis loop in second quadrant

Then, in accordance with the figure, it follows:

$$\frac{B_r}{H_c} = \frac{B_r - B_m}{H_{dem}} \tag{7}$$

Where: B_r – Remanence,

H_c – Coercive force.

$$\frac{B_r}{H_c} = \frac{B_r - B_m}{\frac{B_m}{\mu \cdot \mu_0} \cdot \ln\left(1 + \frac{2\delta}{d_m}\right)} \tag{8}$$

$$B_m = \frac{B_r H_c \mu \mu_0}{B_r \ln\left(1 + \frac{2\delta}{d_m}\right) + H_c \mu \mu_0} = \frac{B_r}{\ln\left(1 + \frac{2\delta}{d_m}\right) + 1} \tag{9}$$

Then, based on the assumption of the linearity of the behavior of the magnetic flux density along the radius:

$$B(x) = \frac{B_r \mu}{\mu_m \cdot \ln\left(1 + \frac{2\delta}{d_m}\right) + \mu} \cdot \frac{d_m}{d_m + 2x} \tag{10}$$

Finite element modeling in Altair Flux was used to verify the obtained results. A simplified diagram of the stator magnetic circuit without stator slots is shown in Figure 27. The Flux model consisted of a SmCo magnet, a 36HXTЮ magnet retaining ring, air gap and a magnetic circuit made of laminated and insulated steel 2421 [29]. The peak of magnetic flux density at a minimum distance from the stator inner diameter was used as a measurement. Flux density distribution in the air gap is sinusoidal.

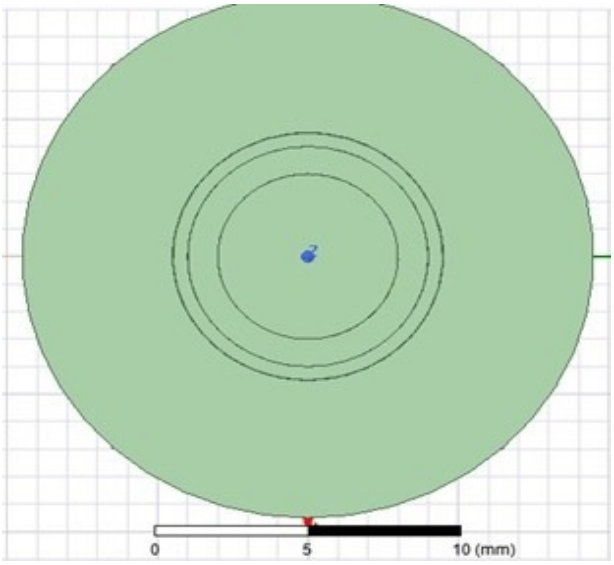

Figure 27: Schema to verify obtained formula

The magnetization curve for electrical steel 2421 is shown in Figure 28. The density of the steel is 7650 kg/m^3, the specific losses at 0.75 T and a frequency of 400 Hz are no more than 10.7 W/kg.

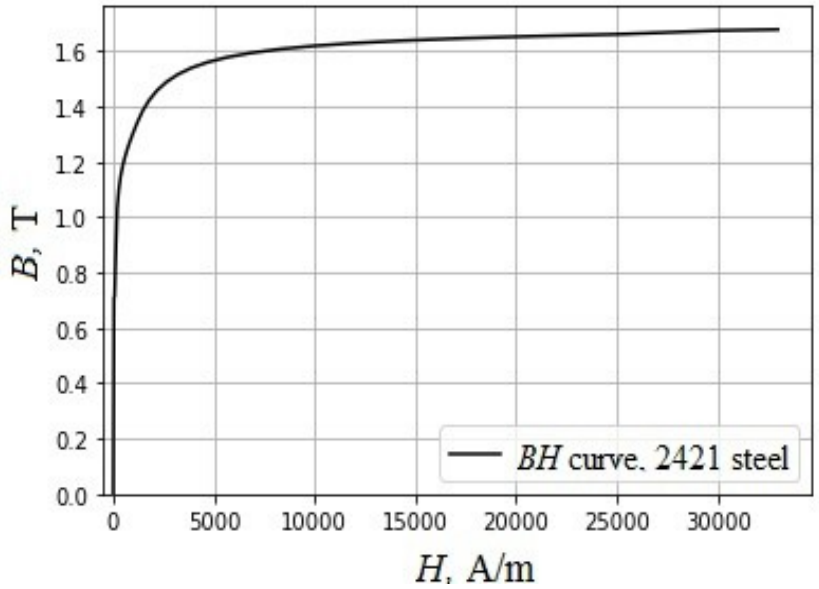

Figure 28: BH curve for 2421 steel (Thickness 0.27 mm with shares of silicon and aluminum)

The verification results for speed 150 000 rpm are shown in Figure 29. In Figure 29, a 5 % deviation from the current value is plotted relative to the calculation in Flux. As can be seen, the resulting model describes well the distribution of magnetic flux density along the radius.

After getting convinced of the applicability of formula (10) in calculating the magnetic flux density in the air gap, we construct the dependence of the magnetic flux density on the diameter of the permanent magnet and the rotor speed, taking into account the results of the strength calculation. For the air gap, we will set the value of 1 mm per side and take into account the thickness of the band. The results obtained with a discrete step 0.1 mm are shown in Figure 30.

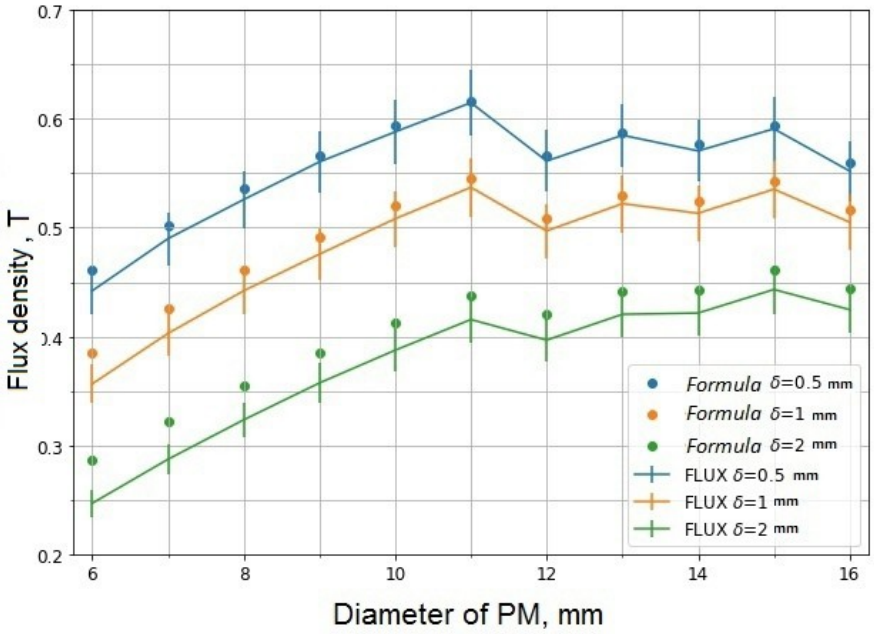

Figure 29: Verification results

Figures 29 and 30 are obtained taking into account the change in the thickness of the magnet retaining sleeve with the change in the diameter of the magnet. The sleeve in equation (10) is modeled by increasing the total effective air gap by the thickness of the sleeve. Sharp jumps on plots in magnetic flux density are associated with an increase in the thickness of the sleeve. For example, in Figure 24 at 150 000 rpm, the thickness of the sleeve begins to grow after a permanent magnet diameter of 11 mm. In Figures 29 and 30, the magnetic flux density after 11 mm drops slightly. Further fluctuations in plots 29 and 30 arise due to different growth rates of the magnet diameter and the thickness of the sleeve.

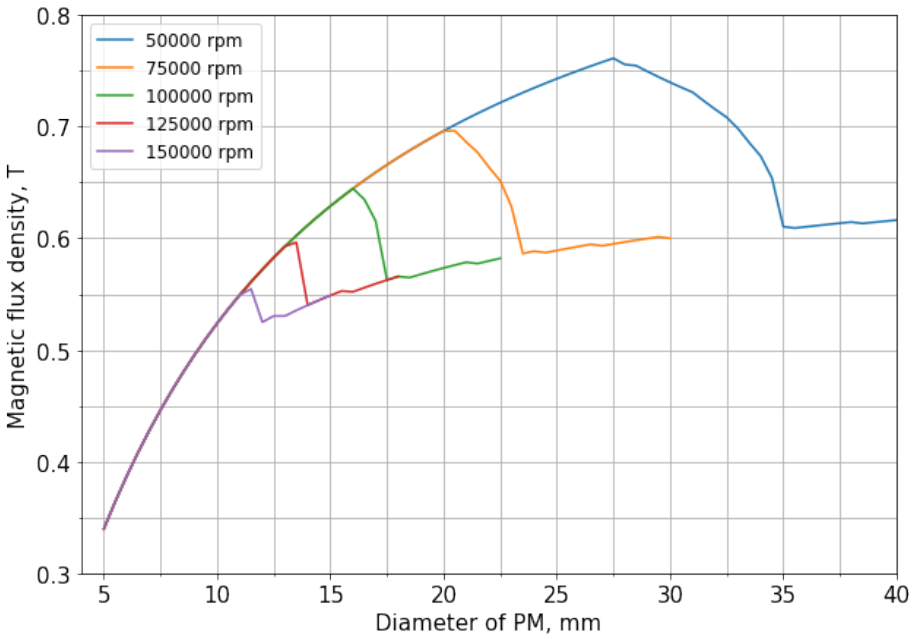

Figure 30: Dependence of flux density on permanent magnet diameter, (Airgap is 1 mm per side)

The resulting plot, based on stress calculations, allows selecting the rotor diameter and magnetic gap, which will provide the reasonable magnetic flux density in the system. It should be noted that it was done without taking into account the effect of the demagnetizing armature reaction.

3.9 Design calculation of the electrical machine

A preliminary structural calculation of a synchronous generator with permanent magnet excitation was carried out using the methodology described in [30].

The power from the turbine shaft was taken as the calculated power from the preliminary design calculation, which is in Appendix 1. This was done to match the design calculations and further simulation of the machine dynamics in Matlab.

As already noticed, the voltage in the DC bus was chosen about 620 V, to be able to form 230 V phase voltage and 400 V line-to-line voltage.

The choice of the diameter of the magnet is challenging. On one hand, an increase in the magnet diameter leads to an increase in the magnetic flux density in the gap, which leads to a decrease in the stator length. On another hand, this can lead to increasing losses in steel, so in this task, it is necessary to understand whether there is an optimum on the parameter range and, if so, where it is.

For these purposes, a program was written. It performs the design calculation of the generator. In this program, the assumption is made about the absence of magnetic flux leakage, as a result of which the magnetic flux density in the yoke elements is 25 % higher than in the calculated model by the finite element method, but still representative and can be used to assess the effect of various parameters on both losses and to other target metrics.

One of the plots responsible for choosing the diameter of the permanent magnet is shown in Figure 31. The potential diameters of the permanent magnet are plotted along the horizontal axis, and the estimated sum of generator iron and Joule losses is plotted along the vertical axis. The corresponding machine mass is shown using color legend.

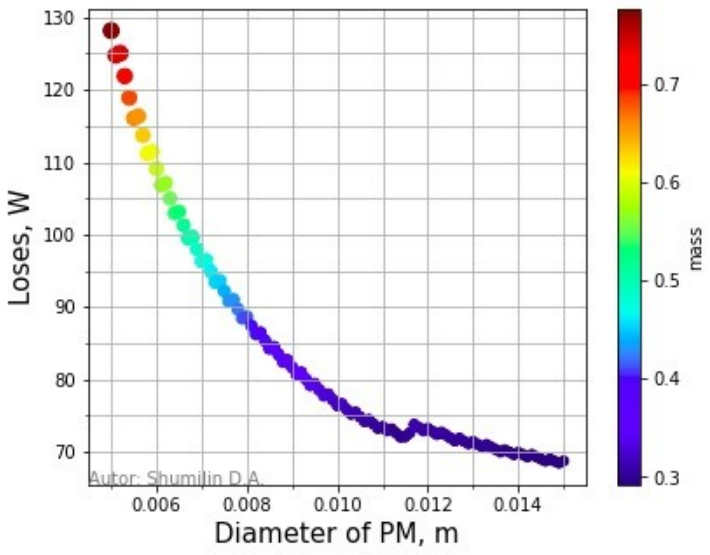

Figure 31: Dependence of losses on PM diameter. Mass value in kg.

Increasing permanent magnet diameter leads to decreasing the sum of generator iron and Joule losses and a decrease in mass. Also in this point, safety factor of the sleeve should be taken in to account. Increasing diameter of the permanent magnet makes losses and mass smaller, but mechanical stability of the sleeve makes worse. Usually in engineering, a safety factor is taken from 2.5 to 1.2, for example, in this case, we take a permanent magnet diameter of 13 mm with a safety factor of 1.6 The plot was built at an assumed linear current load of 25 kA/m, a rotation speed of 150 000 rpm, and a current density of 12 A/mm^2.

In this case, there is no optimum for these parameters. Using Figures 24, 30, and 31, the diameter of the permanent magnet was chosen equal to 13 mm, with a band thickness of 1.5 mm, providing a magnetic flux density in the gap of 0.54 T. The calculation of the electric generator is presented in Appendix 2.

3.10 Possible stator designs

One of the best and widespread, electrical steel for the stator of an electric generator available on the Russian market is steel 2421. Electrical steels are fragile. The manufacture of stators is carried out using electrical discharge cutting while another typical approach is to use

laser cutting. Also, the stator of high-speed machines is small, it makes the laying of the winding in the stator slots difficult. Let us try to find a potential substitute for this steel and improve the design.

To simplify the task of manufacturing and laying the winding, as well as, if possible, reduce losses in steel and the mass of the stator, I tried to use Somaloy powder composite as stator material. Somaloy is used to create soft magnetic products of almost any shape by stamping and sintering. Also, this material allows mechanical processing. This property can, in principle, simplify the fabrication of a tooth-coil stator. Let us take Somaloy Prototyping Material from which workpieces with a diameter of 80 mm and a height of 40 mm are made. Since these workpieces are mass-stamped, a lower price is expected for them than for some special types of this material. All properties of this material can be found in [31].

For further calculations and analysis of their results, let us assume that a generator with a DC bus voltage of 620 V is designed to organize in future an inverter unit with the possibility of creating 380 / 220 V. The winding is a star connected one. Line voltage and phase voltage on generator winding are 460 / 265 V, respectively. Rated load current 1.6 A. That is, in fact, the same parameters as for the designed electric generator in paragraph 3.9.

3.10.1 Somaloy, tooth-coil construction

For these data, I made a design calculation of the generator and carried out its modeling by the finite element method in Altair Flux. As a result of the calculation, it was determined that the diameter of the cylindrical permanent magnet is 13 mm, the outer diameter of the sleeve is 16 mm, the stator inner diameter is 18 mm, the number of slots per pole and phase is equal to one. A short-pitched winding with shortening factor of 1/3 is used. This results in a tooth-coil winding. The number of turns in series per stator winding in the Flux model is 82. The thickness of the tooth is 7 mm. With an assumed current density of 12 A/mm^2, the wire has a diameter of 0.5 mm. The length of the turn was 102 mm in the first approximation. The active phase-to-phase resistance of the winding of the machine is 3 ohms. The filter in the DC circuit had a capacitance of 5.6 μF, and an initial voltage of 630 V.

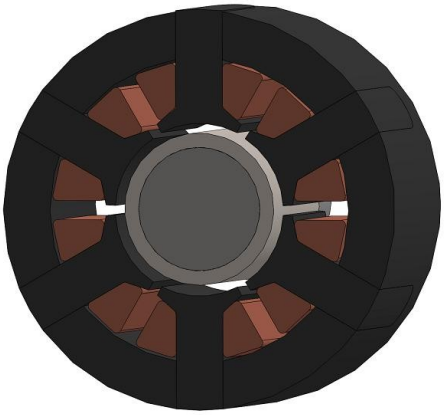

Figure 32: Cross-section cut of Tooth-coil construction

As a result of creating the 3D model shown in Figure 32, the mass of the Somaloy magnetic core was 0.460 kg, the outer diameter was 50 mm.

The open-circuit voltage obtained from the simulation in Flux after a rectifier with a load of 10 000 ohms was 715.7 V.

The peak magnetic flux density in a 7 mm thick tooth was 0.75 T. The peak magnetic flux density in a yoke 7 mm thick was 0.5 T.

Losses in steel, calculated according to Bertotti's method [32], coinciding with the result of calculations according to the formula given in the brochure [31] and equals 67 W. Copper losses equals 12.2 W. The total losses in the stator equal 79.2 W. Specific losses 171.8 W/kg. The efficiency at the rated load was 0.92. The generator phase voltage waveforms are shown in Figure 33.

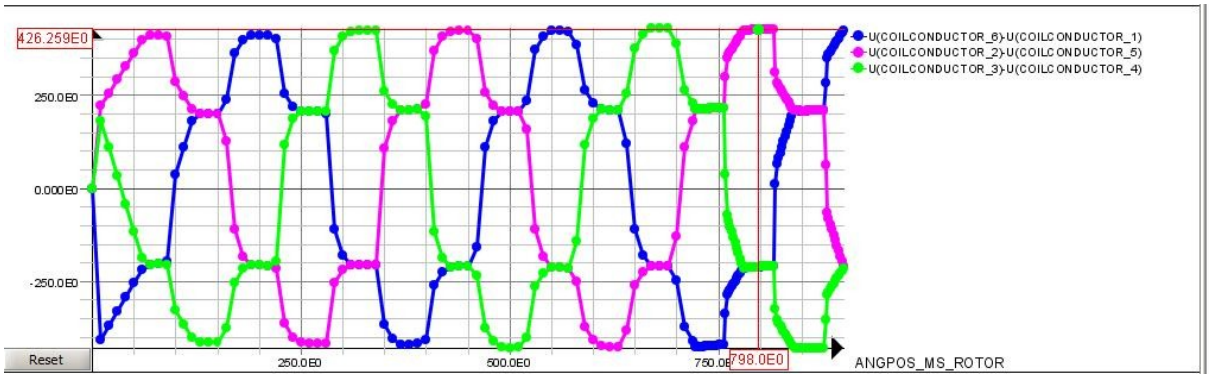

Figure 33: Phase voltages of tooth-coil construction

To estimate the difference in the efficiency of the proposed solution, it is necessary to carry out the calculation of the classical construction of the stator on the same material according to the same algorithm.

3.10.2 Somaloy, classical construction

For the same rotor system, another stator with two slots per pole and phase was designed. A 5/6 shortening factor for a generator of this type allows to reduce the coil inductance and increase the rigidity of the external characteristics of the generator, therefore, in the model, I took a winding short-pitch factor of 5/6. The number of turns in the slot is 38. The thickness of the tooth is 2.2 mm. With an assumed current density of 12 A/mm^2, the wire has a diameter of 0.5 mm. The length of the turn is 240 mm as a first approximation. The active phase-to-phase resistance of the winding of the machine is 3 ohms. The stator section with q = 2 is shown in Figure 34.

The mass of the Somaloy magnetic circuit, modeled in 3D, was 0.179 kg, the volume of the magnetic circuit was 24.53 cm^3. External diameter 38 mm.

The peak magnetic flux density in a 2.2 mm thick tooth was 1.07 T. The peak magnetic flux density in a yoke with a thickness of 4.2 mm was 1.11 T.

The losses, calculated according to the formula given by the manufacturer, were 45.6 W. Copper losses were 11.55 W. The total losses in the stator are 57.15 W. Specific losses 255 W/kg. The efficiency at the rated load was 0.946.

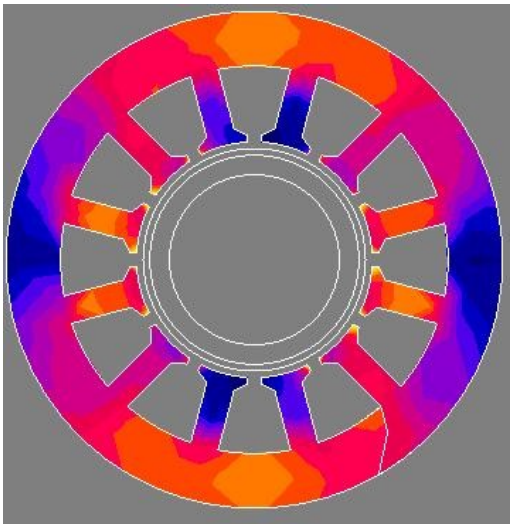

Figure 34: Cross-section view of classical construction, q=2

As can be seen from the presented results, the efficiency in the two stator configurations differs by 2.6 % units, which is a significant reason for rejecting the tooth-coil design and Somaloy material for the developed machine. Looking ahead, I would like to note that the efficiency of an electric generator made of 2421 steel in a classical design is 0.96, which confirms the previous decision.

3.11 Results and characteristics of the generators

Altair FLUX was used to simulate the generator. The constructed 3D model of the magnetic circuit consisted of steel 2421 with the number of turns in the slot equal to 36. Thus, the length of the turn is 225.64 mm in the first approximation. The active phase-to-phase resistance of the winding of the machine is 2.81 ohms. The computational model is shown in Figure 35, the machine mesh is shown in Figure 36.

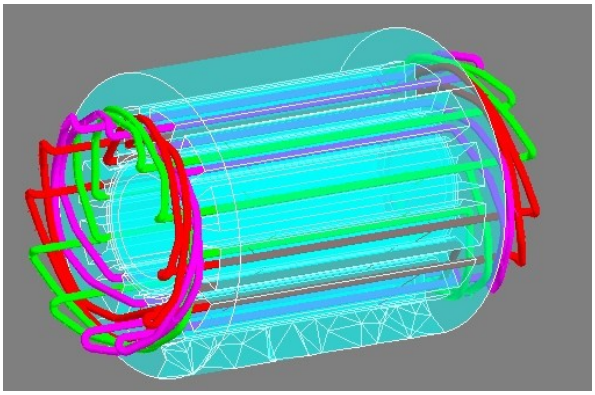

Figure 35: Model of the stator

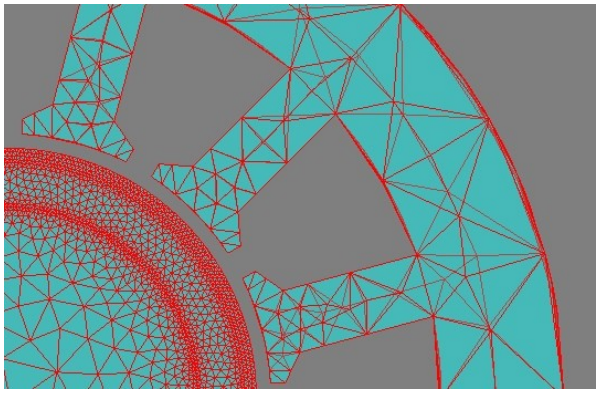

Figure 36: FEM model of the machine

As a result of the calculation, the mass of the magnetic circuit was 0.19 kg. The peak magnetic flux density in a 2.2 mm thick tooth was 1.08 T. The peak magnetic flux density in a yoke with a thickness of 4.2 mm was 1.12 T. The loss in steel, calculated using the Bertotti method, was 28 W. Copper losses were 11 W. The total losses in the stator are 39 W. Specific losses are 147 W/kg. The efficiency at the rated load was 0.96. Figures 37 and 38 show the distribution of magnetic flux density over the stator volume.

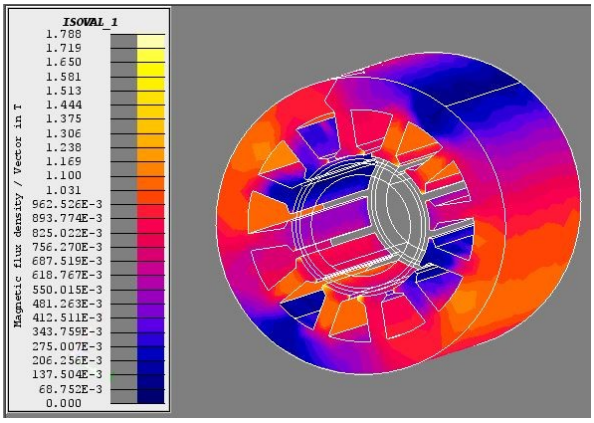

Figure 37: 3D distribution of flux density over the model

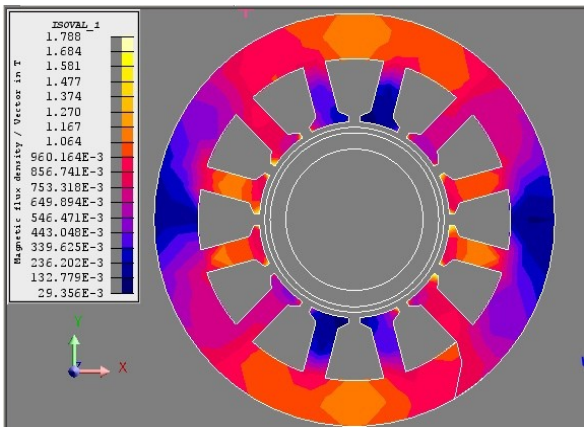

Figure 38: 2D distribution of flux density over the model

Using the previously obtained results and the accepted values, it is possible to obtain a more accurate mass of the stator with the copper winding (Figure 39). A plots of the phase voltages and currents of the generator are shown in Figure 40 and Figure 41. Machine characteristics can now be evaluated.

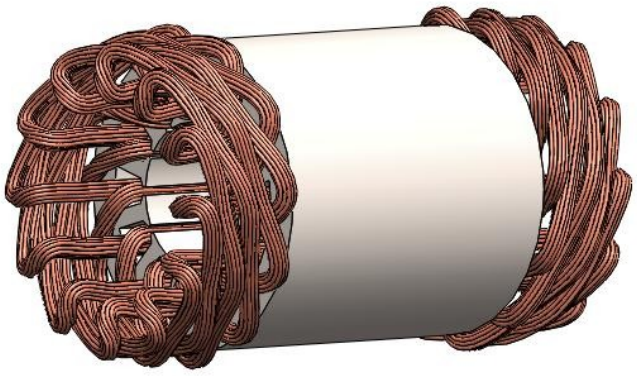

Figure 39: Stator 3D model with winding

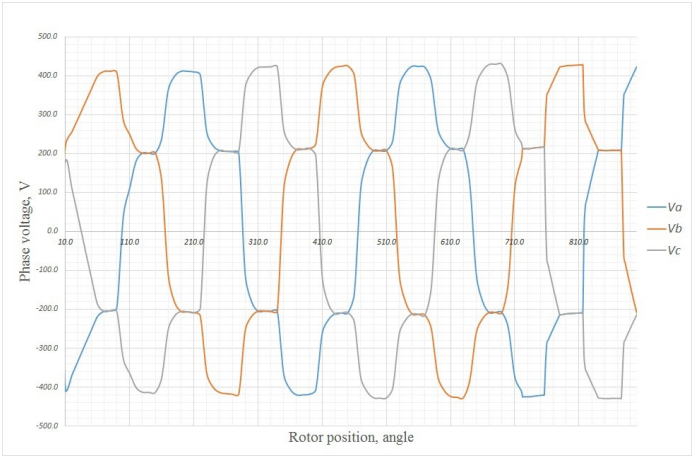

Figure 40: Phase voltages

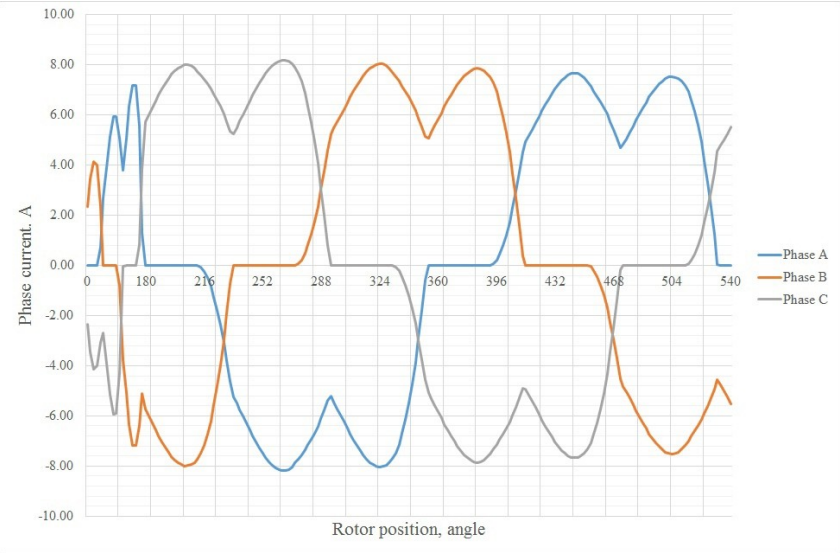

Figure 41: Phase currents

The constructed 3D model of the stator magnetic circuit using SolidWorks is shown in Figure 39. In the model, the entire winding is drawn in the form of loops, but this approach still allows us to fairly accurately estimate the mass of the winding. The mass was 0.27 kg, the coil length was 240 mm.

Finite element calculations in Altair Flux can be carried out sequentially one after another in automatic mode. This circumstance makes it possible to easily obtain characteristics of the electric machine. Four calculations with constant DC capacitance of 5.6 μF were made to build characteristics:

a) The open-circuit voltage measured after the rectifier with a load of 1 000 000 ohms was 739 V;

b) The voltage across the 667 Ohm load was 631 V. Load current 0.95 A. Thus, the power was 597 W;

c) The voltage across the 385 Ohm load was 620 V. The load current is 1.61 A. Thus, the power was 1000 W;

d) The voltage across the 200 Ohm load was 594 V. The load current was 2.97 A. Thus, the power was 1760 W.

For the future simulation of the dynamic processes of the turbine generator, from the calculation performed in Flux, the characteristics necessary for specifying a permanent magnet excited synchronous generator in the Matlab Simulink environment were obtained, namely, the phase inductance equal to 0.81 mH and the magnetic flux of 24.9 mWb.

Based on the data obtained using simulation in Flux, characteristics were built using Matlab Simulink to estimate the applicability of the synchronous generator model in Simulink in the generator's dynamic processes.

Characteristics are presented on Figure 42.

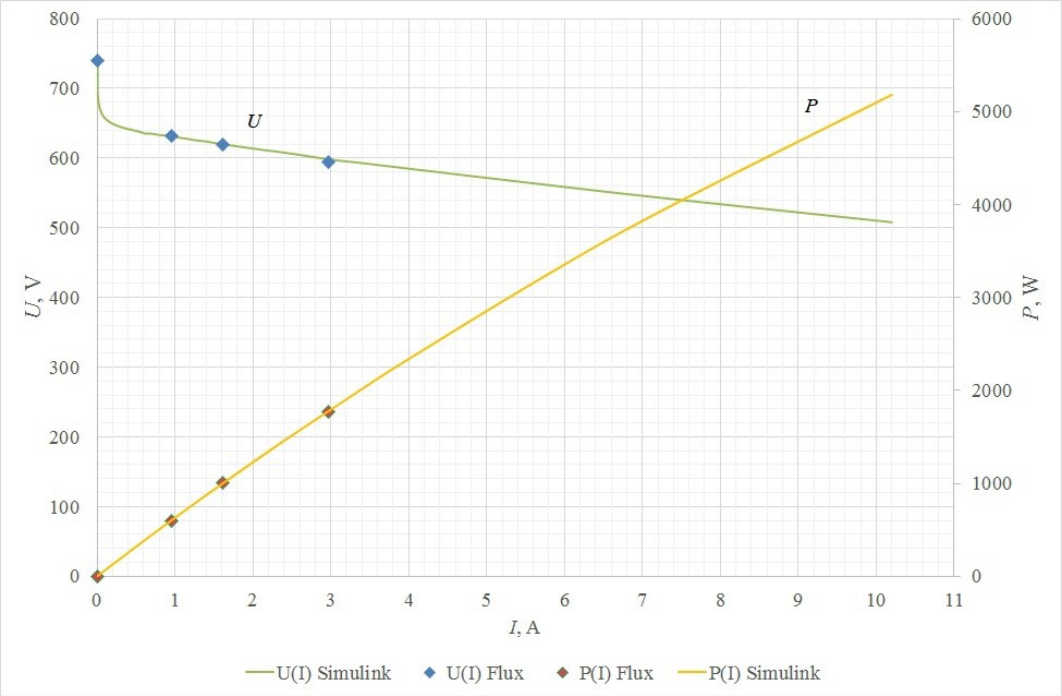

Figure 42: Characteristic curves for synchronous machine with permanent magnet

As can be seen in Figure 42, the dependencies of voltage and power on load current coincide. Thus, it can be concluded that the basic model of a permanent magnet synchronous machine can be used to simulate a dynamic process.

3.12 Rotor system strength calculations

The rotor is the most critical and mechanically heavily loaded part of the turbogenerator unit. As it was already described earlier, the rotor consists of a permanent magnet (SmCo5), a bandage (steel 36HXTIO) which is longer than the permanent magnet. The bandage is fitted on the permanent magnet with a calculated shrink fitting. To fix the rotor in space, steel pins are installed at both ends, to which the bandage is welded. A steel disk is located on the front pin to allow using thrust gas-dynamic bearing. The turbine impeller, made of 6061 T6 aluminum alloy, is screwed onto the front pin in the direction of rotation, preventing unscrewing during normal operation of the machine. The rotor design is shown in Figure 43.

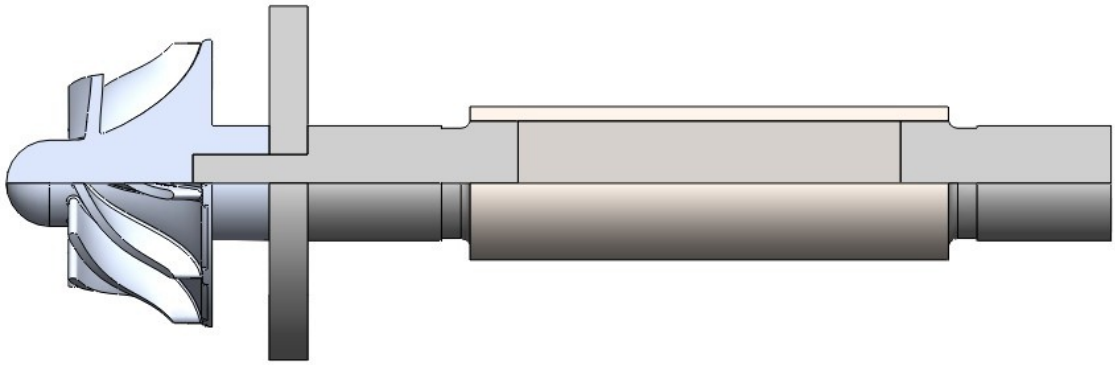

Figure 43: Rotor system

The system presented in Figure 43 was modeled during calculation stress by the finite element method. The boundary conditions were sliders on the pins, which simulated bearings, as well as a slider on one disk side to simulate the thrust bearing limitation. The rotor rotated at a frequency of 150 000 rpm. As an additional load, the retaining ring fitting on the permanent magnet was set by simulating the mutual displacement of the contact surface towards the magnet. The main purpose of this calculation was to test the system, in particular, to test the stress in the retaining ring-magnet part. Figure 44 shows the stress distribution over the surface of the rotor system.

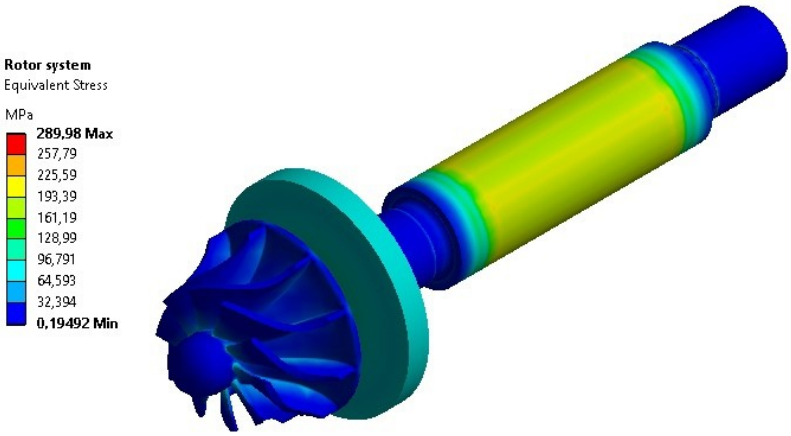

Figure 44: Stress distribution in rotor system

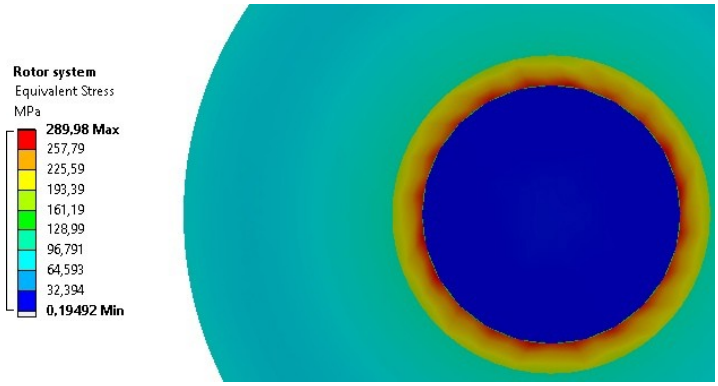

Figure 45: Rotor cross-section view

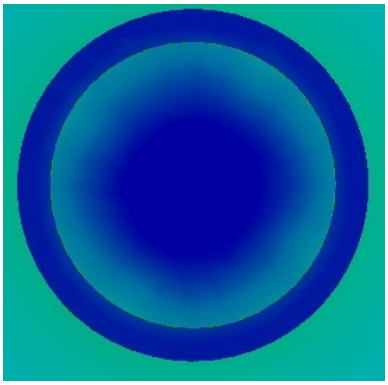

Figure 46: Rotor cross-section view close to the pin

As expected, the greatest stresses occurred in the bandage at the contact surface between the bandage material and the magnet. The stress distribution over the retaining ring and the magnet in its center are shown in Figure 45. The stress distribution over the magnet near the pin surface is shown in Figure 46. It can be noticed that the stress in the permanent magnet is compressive or close to zero, which corresponds to the designing idea and ensures the reliability of the permanent magnet throughout the operating range. The safety factor for the band is quite high.

3.13 Rotor vibration diagram

Since the rotor of the machine rotates at 2500 revolutions per second, there is a possibility that the rotor will pass through the natural frequencies of the rotor when the machine is started. There is also a possibility of designing a rotor that will have an operating frequency close to the natural frequency of oscillations at the nominal operating mode, which is unacceptable. For this, using the model given in paragraph 3.12, the natural frequencies of the rotor system were calculated and a vibration diagram was built (Figure 47). The calculation was based on the vibration estimation technique for turbine blades described in [33].

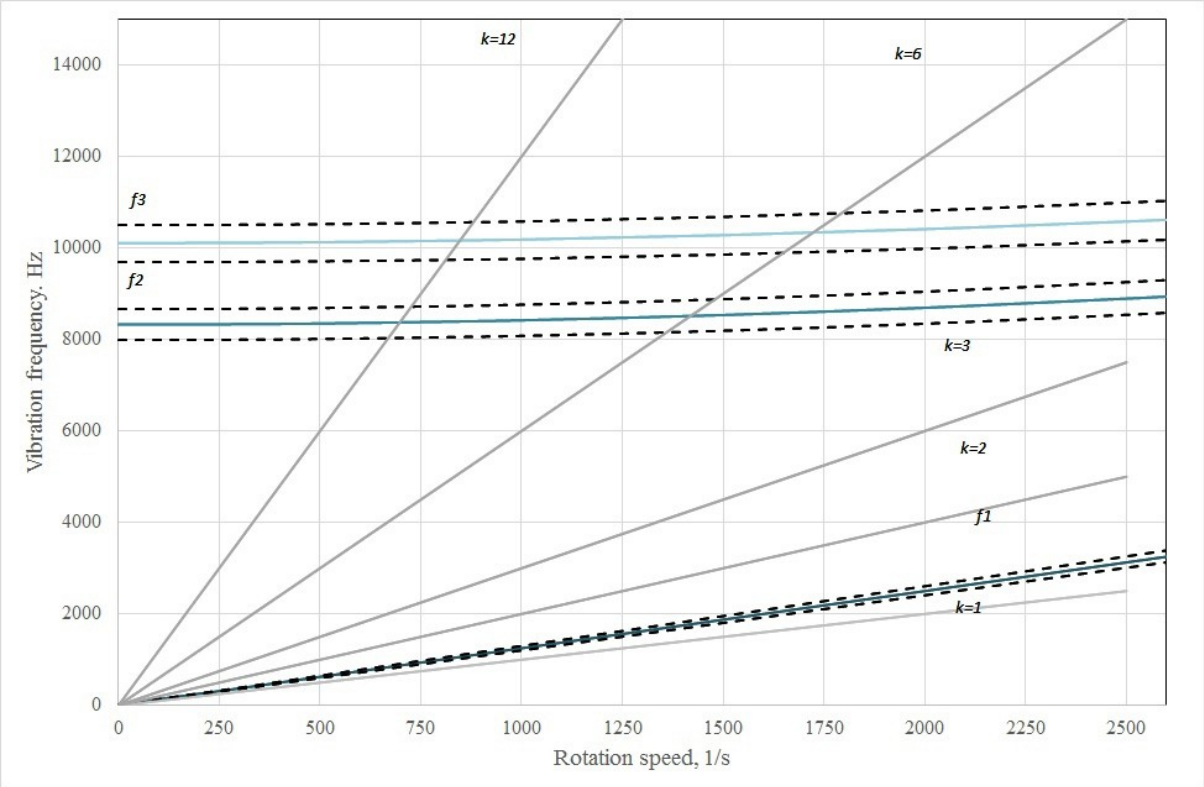

Figure 47: Vibration diagram

On the plot *f1* is the first natural frequency of oscillations, *f2* is the second, and *f3* is the third. Further frequencies are too high and do not fall into the interesting and close to nominal operation region. The gray lines show the frequency of exposure as multiples of *k*. Since the potential multiple frequencies can be 2, 3, as well as 6 (the number of nozzle channels), 12 (the number of slots in the magnetic circuit), then these lines are shown in Figure 47. The intersection of the range ±4 % of the natural frequency of oscillations and lines *k* gives a potentially dangerous range of the rotor operation, which must be passed during start as quickly as possible.

In Figure 47, the intersection of lines *k* and *f* does not occur in the area close to the nominal rotor speed. At the first start of the turbine unit, you should especially carefully monitor the state of the system in the ranges from 600 to 1000, as well as from 1300 to 1800 revolutions per second.

3.14 Summary

This chapter describes approaches to the design and analysis of high-speed, low-power turbogenerators. As result, an axial-radial turbine with an internal efficiency of 86.2 % and a favorable flow of the working fluid inside the flow path was obtained. In addition, the calculation and simulation of the permanent magnet synchronous generator were performed. The resulting generator has an efficiency of 96 %. The retaining ring and the permanent magnet in the center of the rotor withstand the loads at nominal operating conditions. The rotor system is reliable. Rated rotor speed is not in the range of natural frequencies.

4. Basic control system

4.1. Concept of the control system for the turbogenerator

To create autonomous heat and electricity energy generators, it is necessary to make a reliable automation system for starting and maintaining the system operation. For low-power turbogenerators, the nominal pressure creates a large axial force, which presses the heel of the thrust foil gas-dynamic bearing to the housing, creating a large dry friction torque that prevents the machine from accelerating. The situation becomes worse because a useful start torque on the impeller is very low for low-power machines since the rotor speed is high. All this leads to the fact that it naturally becomes impossible to starting low-power turbogenerators on foil gas-dynamic bearings. A possible solution to this problem is to operate the generator as a motor. The source of energy can be either a storage battery installed in the DC bus of the electronic converter, or an AC network with an additional electronic setup in the case of the installation in parallel with this network. In the starting mode, the phases of the electric machine are connected to the voltage inverter, and the rotor of the machine is accelerated to a given pick-up frequency. After reaching the pick-up frequency a gas is supplied to the turbine, the same inverter can be switched to the active rectifier mode to rectify the turbogenerator voltage, stabilize the DC bus voltage at 620 V to simplify the operation of a subsequent inverter.

The rotor speed during operation should not deviate from the rated value. Since the rotational speed is high and the rotor is mechanically heavily loaded, the creation of frequent additional dynamic forces on the rotor system (for example, the impact of the flow from nozzles on the rotor) will lead to a significant reduction in the hours of the normal operation of the machine. Since the moment of inertia of the rotor is small, the acceleration of the rotor will be rapid. Therefore, the system for maintaining the necessary parameters of the working fluid must be made in the form of an electronic control system. Hydraulic control systems which are currently used can regulate the steam flow into large and powerful turbines. Another argument in favor of a constant rotor speed is the presence of potentially dangerous regions in terms of rotor vibration. The operation of the machine in a vibration-hazardous zone is prohibited.

The installation must contain at least two valves. The one closest to the turbine is the control valve, which regulates the mass flow of the working fluid into the turbine flow path. The second is a shut-off valve for instantaneous blocking access of the working fluid to the

turbine flow path. In all turbines, it is accepted that the overshoot of the rotor speed should not exceed 10 % of the nominal speed. If the frequency is exceeded the shut-off valve must close the access of the working fluid to the flow path. The turbine control system should be designed in a way that the overshoot of the speed of more than 10 % does not occur after full load shedding.

The power electronics unit, which consists of an active rectifier that can operate in the inverter mode, maintains the voltage in the DC bus at an almost constant voltage during normal operation, which makes it possible to simplify the program logic of the subsequent inverter. The inverter from the 620 V DC bus generates the required voltage and frequency for the consumer. The DC bus also charges the starting battery.

4.2. Matlab simulation model

To estimate the overshoot of the rotational speed at the start of the machine and during load shedding mathematical model of the turbogenerator was built in Matlab Simulink.
The model is shown in Figure 48.

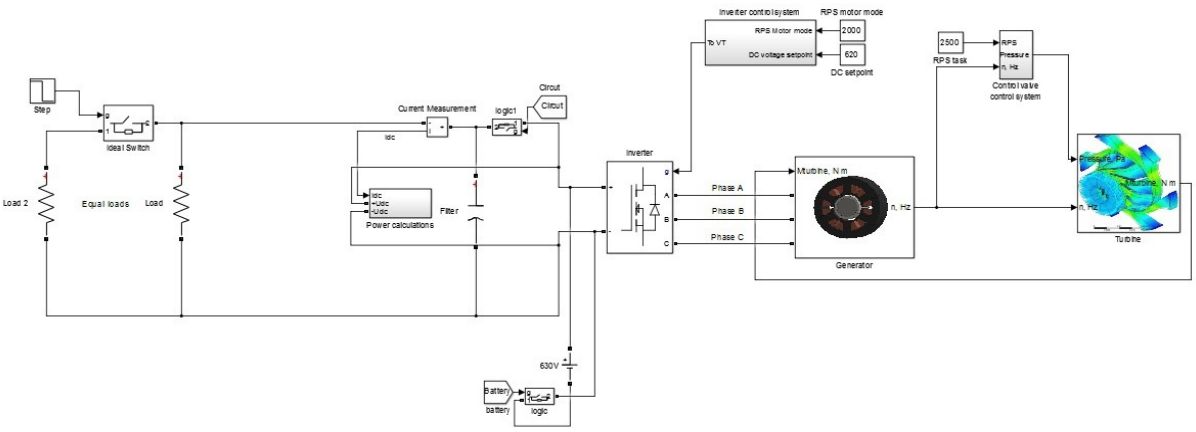

Figure 48: Model of the turbogenerator

The model consists of many blocks. I will describe only the main ones.

The turbine block in Figure 48 is labeled "Turbine". The turbine is modeled by direct calculation of the turbine flow path with fixed geometric parameters corresponding to the result from Appendix 1. The basic computation is based on the sources [14, 16]. Since in the process of changing the rotational speed, the gas-dynamic parameters also change, the blocks describing the variable operation of the turbine were built into the turbine model according to [34]. To describe the variable operation modes extra blocks were added for recalculating the

mass flow rate and the degree of reactivity of the stage. Since the turbine unit was created specifically for testing on the gas-dynamic setup described in Chapter 2, the dependence of the outlet pressure from the turbine on the flow rate of the working fluid was added to the turbine block in the form of an approximated polynomial equation. Since the geometry of the machine is already known, additional frictional torque from the rotor of the generator was added to the turbine block. The rotor of the generator creates additional ventilation losses. A mathematical expression for calculating losses can be found in [35]. In structure, the block transmits the torque for the electric generator after subtracting the significant frictional torque by the rotor ventilation from the total input torque.

The block of the electric generator consists of a model of a permanent magnet synchronous generator predefined in Matlab. The rotor moment of inertia was set to $993 \cdot 10^{-8}$ kg·m^2. The moment of inertia was obtained by building a 3D rotor model shown in Figure 42 and calculating using the built-in SolidWorks tools under all given model materials. The phase resistance is set as 1.4 Ohm, the stator phase synchronous induction is set at $0.81 \cdot 10^{-3}$ H. As it was shown earlier in paragraph 3.11, the generator block is in good agreement with the calculated model in Flux. The generator block in Figure 48 is represented by a block labeled "Generator".

The inverter unit (active rectifier) is controlled by the vector control system either for the motor mode and for the mode of maintaining constant voltage value in the DC bus. The vector control system is implemented according to the method described in [36]. The selected switching frequency of the keys is 50 kHz. In Figure 48, the block is represented by the name "Inverter control system". Despite the fact that the inverter is shown created using IGBT keys, this is an example. Designing of the power electronic unit is not a part of this work.

The turbine control system is represented by the block "Control valve control system". The control system is based on a PI regulator and operates by using error between desirable speed and current speed. The PI regulator controls the initial pressure at the turbine inlet. It is limited at the top by a pressure of 3.5 bar to prevent excessive acceleration of the rotor at higher pressures and thus higher mass flow rates. This PI regulator can serve as a very simple simulation of a servo-driven control valve that transmits force to the valve through a mechanical transmission. The rotor speed control system must be fast to prevent overshooting.

When starting from the standstill, the turbogenerator accelerates in motor mode from a 630 V constant voltage source (battery). When the rotor reaches a rotational speed of 2000 Hz, using the logic block, the battery is disconnected from the inverter. After that, the

inverter goes into rectifier mode and is connected to the load. In DC-link of the inverter, a capacitor with a capacity of $5.6 \cdot 10^{-6}$ F. is installed. Figure 48 also shows the load, for example, in the form of two parallel resistors with a resistance of 762 Ohm each.

To simulate the rotor acceleration and load shedding, a slightly modified scheme was used. It is shown in Figure 49. In this figure, the load is shown by one resistor, which can be disconnected from the machine using an additional key logic2 While simulating a full load shedding from a turbogenerator, the model is disconnected from the load using the logic2 key, and the speed rapidly increasing. Full load shedding occurs from the nominal parameters simulating the worst-case scenario when the nominal mass flow and rotation speed of 150 000 rpm are still supplied to the turbine.

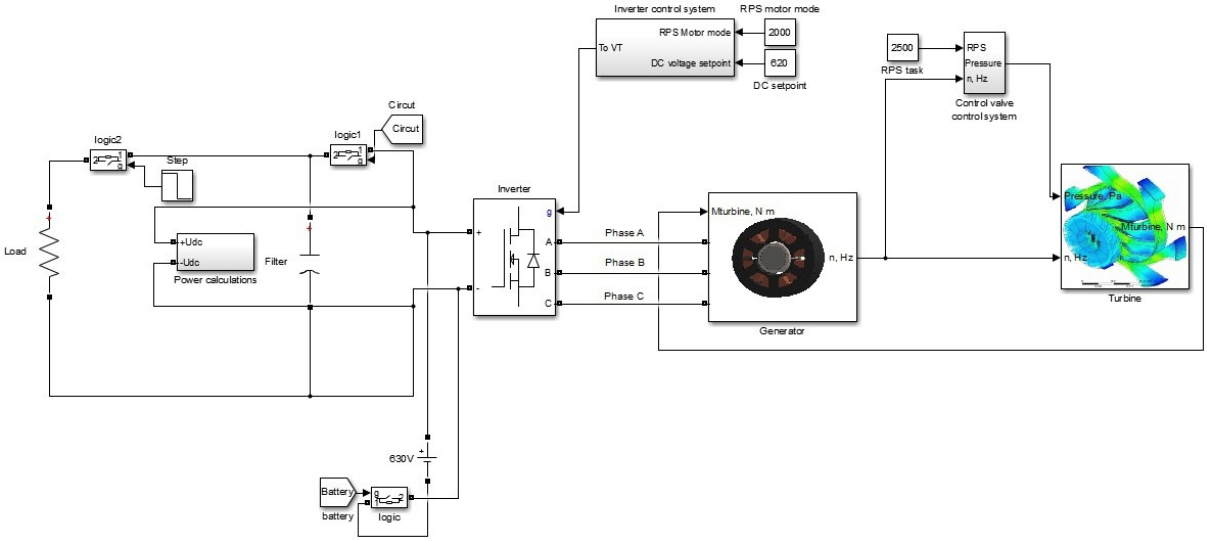

Figure 49: Model to simulate the full load shedding

4.3. Modeling results

As a result of the simulation, plots of the machine starting from the state of rest to the nominal operating mode and the full load shedding were obtained.

Figure 50 shows a plot of the reaching of the machine to the rated design parameters. Assuming that there are no frictional forces in the bearings of the machine, the machine in motor mode is capable of gaining 2000 revolutions per second in 2.06 seconds. Further, in the generator mode, the machine reaches its nominal parameters in about 3 seconds. The overshooting of the speed does not exceed 10 % and was 1.5 % for the designed system.

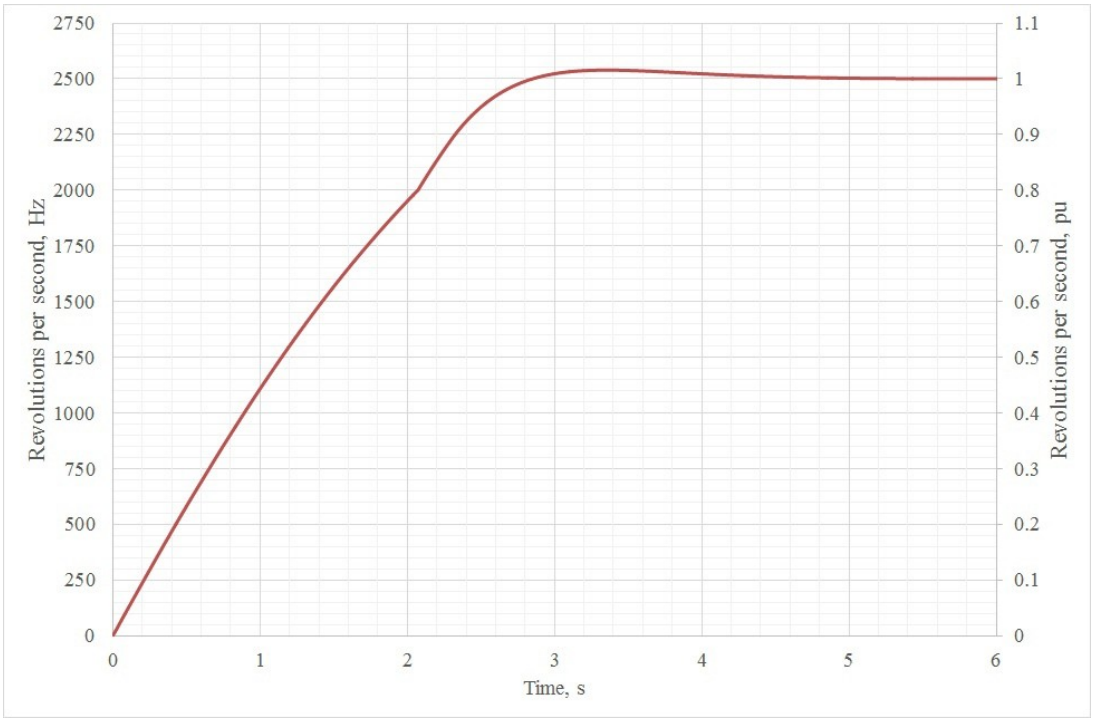

Figure 50: Acceleration of the turbogenerator

Figure 51 shows a plot of overshooting at full load shedding. Load shedding occurred at the moment of 1 second. The control system is able to handle this task and allows to keep the rotor from accelerating by more than 10 %. The overshooting of the rotational speed was 7.3 %. The time it takes for the rotor to return to the rated speed is about 4 seconds.

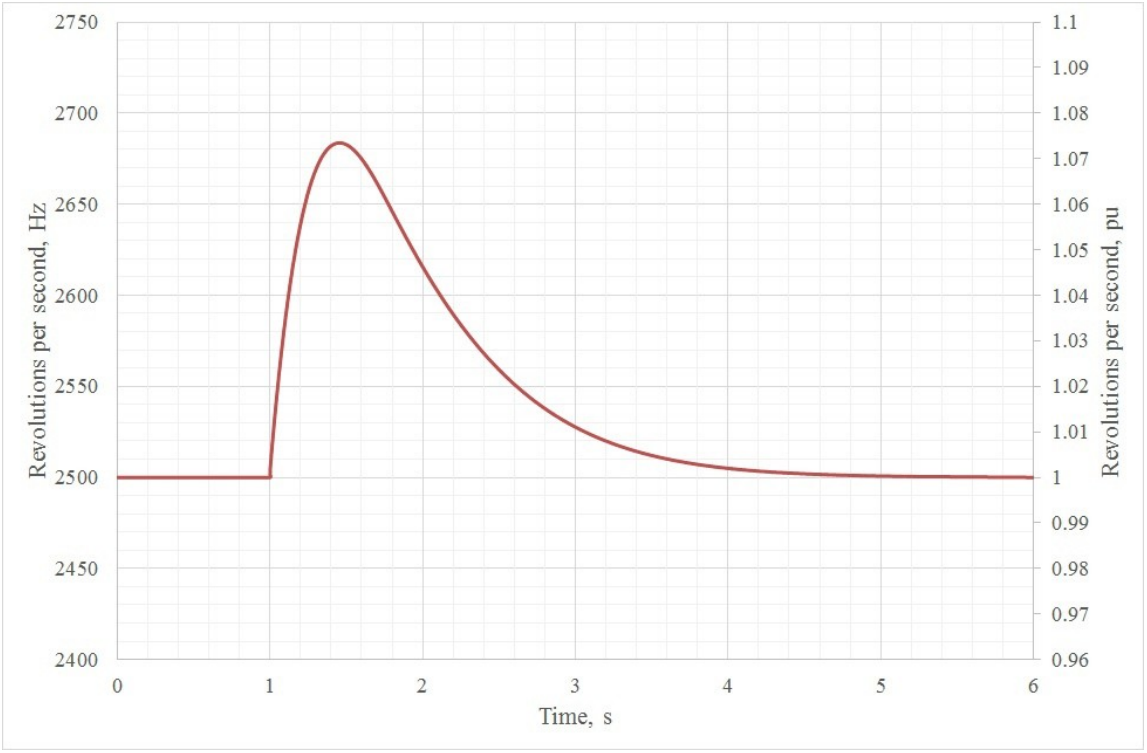

Figure 51: Simulation of full load shedding

5. Conclusions

The designed turbogenerator is an experimental unit to investigate processes in high-speed machines. The approach presented in this work makes it possible to design various types of machines and test them on gas-dynamic test stands. The obtained parameters and characteristics of gas-dynamic processes in the machine can be recalculated according to the theory of similarity for full-scale objects. Full-scale objects can also be air turbogenerators and machines with other working fluids, including units based on organic fluids.

Machines similar to the one designed can be used e.g. as part of organic Rankine cycle as a waste heat utilizer. Another option of the use such a generator is to build a gas turbine including a compressor on the same shaft.

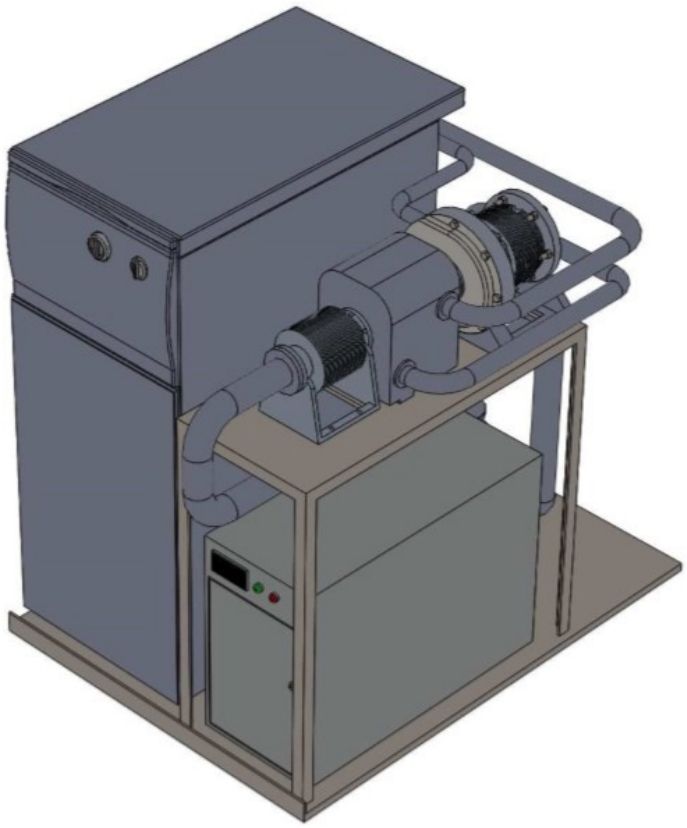

Figure 52: Concept of the power plant with designed turbogenerator

For example, waste-heat recovery system can utilize the heat of exhaust gases from power boilers (the temperature of which do not exceed 120-150 degrees Celsius). Another example would be the use of exhaust heat from diesel engines to generate electricity. Diesel engines are used widely in power production, in ships in heavy transport systems like diesel locomotives and so on. The generated electricity could be used e.g. in heating devices in a railway carriage.

Also, the machine can be part of an autonomous power plant to generate heat and electricity. The concept of such an plant is shown in Figure 52. On figure depicted an autonomous low power plant operating on pellet biofuel. Potentially, such plants can be mobile and almost do not require maintenance only refueling. The schema of this unit is completely consistent with Figure 7 from Chapter 1.

An additional area of application for such machines is pressure-lowering power plants or starter motors. For example, additional power generation onboard an aircraft by draining air from aircraft engines.

In the master's thesis a high-speed low-power turbogenerator for the parameters of 150 000 rpm with a power of 1000 W was designed. The efficiency of the machine is 80.5 %, the mass is estimated at 3 kg. The machine dimensions are 168 mm long and 132 mm in diameter at the widest part of the unit. The appearances of the designed turbogenerator are shown in Figures 53 and 54. A 3D detailed model of the machine in SolidWorks was designed.

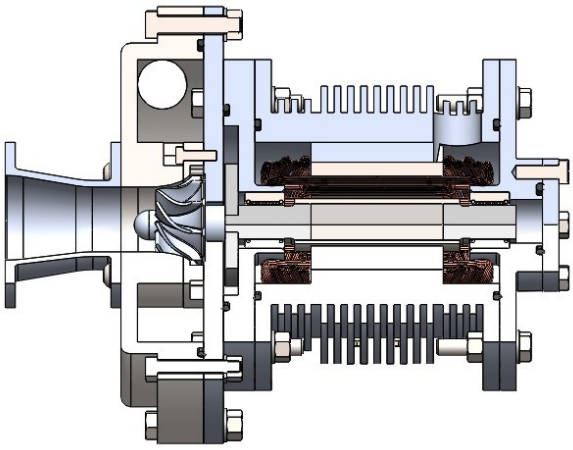

Figure 53: Side view of the turbogenerator

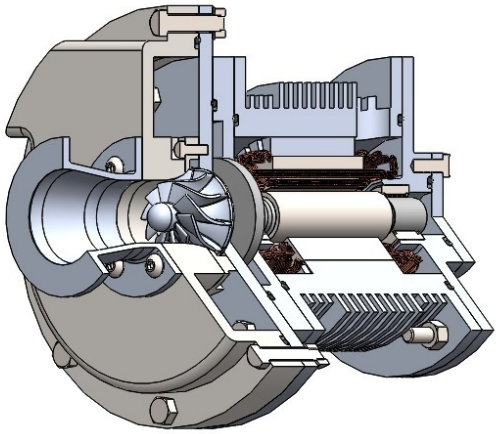

Figure 54: 3D view of the turbogenerator

Figure 55 shows a combined plot of the acceleration of the machine in the start-up mode and the speed overshooting after possible load shedding. The simulated control system ensures that the machine reaches its nominal parameters with an overshoot of 1.5 %. Acceleration from standstill takes approximately 4 seconds. Also, the control system can handle keeping the speed from overshoot. The turbogenerator without load, at the nominal parameters of the working fluid, provides an increase in the rotor speed by 10 % in a time of about 0.5 seconds.

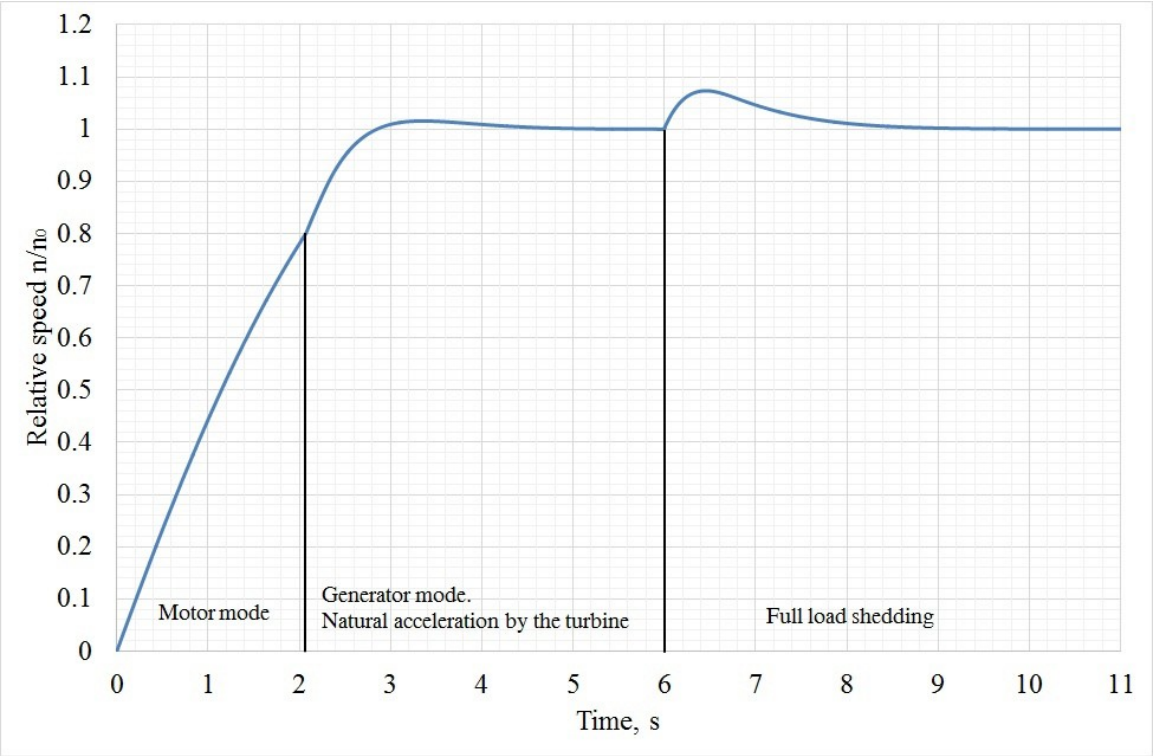

Figure 55: Dynamics simulation result

As a result of the master's thesis, an experimental low-power air turbine unit was designed. Calculations and optimization of the turbine flow path were carried out, as well as modeling of the flow in the flow path using the finite element methods. A theory for estimating the magnetic flux density in an air gap, taking into account the strength of the magnet-sleeve system, has been developed and verified with calculations by a numerical method in Altair Flux. Calculations and optimizations of various designs of a permanent magnet synchronous generator were carried out. The resulting machines were simulated in Altair Flux using finite element methods and the best one was chosen. With the obtained geometry of the machine, a detailed 3D model was designed, and its mass and dimensions were estimated. Having a rotor model, the strength calculation of the rotor system was carried out, showing that the rotor meets the reliability requirements. Also, the natural frequencies of the rotor oscillations were obtained, and the vibration diagram was built. The nominal rotor speed is far away from vibration-hazardous zones. With the available design parameters, a model in Matlab Simulink was developed to estimate the start-up time of the machine. In addition, complete load shedding from the machine was simulated using the model. Speed overshooting of the rotational speed during load shedding does not exceed 10 %.

Based on the work, it is now possible to build a real prototype and test it on the test stand described in the work.

References

[1] Eurostat, 2020, “Energy, Transport and Environment statistics”, 2020 edition, Luxembourg: Publications Office of the European Union, doi:10.2785/522192 KS-DK-20-001-EN-N

[2] Leoncini, Lorenzo. (2019). European Union energy trends from 2020 to 2050. [Cited 3 February 2021]. Available at: https://www.researchgate.net/publication/335840713_European_Union_energy_trends_from_2020_to_2050

[3] Forecast for the development of energy in the world and Russia 2019. ed. A.A. Makarova, T.A. Mitrova, V.A. Kulagin; ERI RAS, Moscow School of Management Skolkovo. Moscow. 2019. ISBN 978-5-91438-028-8

[4] Tartière T, Astolfi M. A World Overview of the Organic Rankine Cycle Market. Energy Procedia Available from: http://dx.doi.org/10.1016/j.egypro.2017.09.159

[5] Capstone Turbine Corporation. C30 Engine Components. [Cited 19.12.2020] Available at: https://d1io3yog0oux5.cloudfront.net/_af40c47cd833ba21830650a9fb53c15a/capstoneturbine/db/235/9436/file/C30+Renewable+Fuels.pdf

[6] Exergy. The innovative radial outflow turbine. [Cited 19.12.2020] Available at: https://www.exergy-orc.com/upload/pages/283/exergy-brochure_corporate_EN.pdf

[7] Heat recovery solution. Integrated power module. [Cited 20.12.2020] Available at: http://heatrecoverysolutions.com/cleancycle

[8] Wu, Meng. “Design and Performance Analysis of a Radial Inflow Turbogenerator with the Aerostatic Bearings for Organic Rankine Cycle System.” Energy Conversion and Management, vol. 214, Elsevier Ltd, June 2020, p. 112910–, doi:10.1016/j.enconman.2020.112910.

[9] Grönman, Aki, et al. Design and Verification of a Hermetic High-Speed Turbogenerator Concept for Biomass and Waste Heat Recovery Applications. Elsevier, Sept. 2020.

[10] Saleh, Bahaa & Koglbauer, Gerald & Wendland, Martin & Fischer, Johann. (2007). Working fluids for low-temperature Organic Rankine Cycles. Energy. 32. 1210-1221. 10.1016/j.energy.2006.07.001

[11] Sylvain Quoilin, Martijn Van Den Broek, Sébastien Declaye, Pierre Dewallef, Vincent Lemort. Techno-economic survey of Organic Rankine Cycle (ORC) systems, Renewable and Sustainable Energy Reviews, Volume 22, 2013, ISSN 1364-0321

[12] M. Rumyantsev, D. Shumilin, "Automated Complex for Researching High-Speed Electric Turbomachines," 2020 V International Conference on Information Technologies in Engineering Education (Inforino), Moscow, Russia, 2020, pp. 1-4, doi: 10.1109/Inforino48376.2020.9111750.

[13] Wikipedia contributors. "Specific speed." [Cited 21.04.2021] Available at: https://en.wikipedia.org/wiki/Specific_speed

[14] A. G. Kostyuk, A. E. Bulkin, A. D. Trukhny. “Steam and gas turbines for power plants” Moscow. MPEI Publishing House, 2019. - ISBN 978-5-383-01400-4

[15] A. M. Arkharov, I. A. Arkharov, A. N. Antonov and others. “Low temperature machine technology. Cryogenic machines and instruments”: Publishing house of MSTU named after N.E. Bauman, 2011.

[16] A.E. Zaryankin, A.N. Sherstyuk. “Small-scale radial-axial small-power turbines” Mashgiz, Moscow, 1963.

[17] Alnico magnets of the group of companies "North-West Laboratory" [Cited 19.12.2020] Available at: http://ferrite.ru/products/magnets/alnico/

[18] GOST 24897-81 [Cited 19.12.2020] Available at: http://docs.cntd.ru/document/gost-24897-81

[19] Deformable magnets of the SpetsMagnet company [Cited 19.12.2020] Available at: http://s-magnet.ru/постоянные-магниты-производитель/деформируемые-магниты/

[20] Powder magnets of the Spetsmagnit company [Cited 19.12.2020] Available at: http://s-magnet.ru/постоянные-магниты-производитель/спеченые-порошковые-магниты-из-редк/

[21] GOST P 52956-2008 [Cited 19.12.2020] Available at: http://docs.cntd.ru/document/1200066645

[22] Magnetron neodymium magnets [Cited 19.12.2020] Available at: http://tdmagneton.ru/redkozemelnyie-nefebr

[23] A.P. Tyutnev, V.V. Sergeev, V.T. Semyonov, G.P. Stanolevich. On the issue of radiation resistance of permanent magnets based on rare earth elements. Electromechanical issues. VNIIEM Proceedings. Publ .: Research and Production Corporation "Space Monitoring Systems, Information Control and Electromechanical Complexes" named after A.G. Iosifyan

[24] Magnetron based SmCO magnets [Cited 19.12.2020] Available at: http://tdmagneton.ru/redkozemelnyie-smco

[25] SmCo magnets of the North-West Laboratory group of companies [Cited 19.12.2020] Available at: http://ferrite.ru/products/magnets/smco/

[26] GOST 14117-85 [Cited 21.04.2021] Available at: https://docs.cntd.ru/document/1200009117

[27] I.A. Birger, B.F. Shorr, G.B. Iosilevich. Strength calculation of machine parts: Handbook. 4th ed. Moscow, 1993.

[28] Sugrobov A.M., Rusakov A.M. Designing electrical machines of autonomous objects: a textbook for universities. MPEI Publishing House. Moscow. 2012.

[29] GOST 21427.2-83 [Cited 21.04.2021] Available at: https://docs.cntd.ru/document/1200009104

[30] V.A. Balagurov. Designing Special AC Electric Machines: A Textbook for University Students. Higher school. Moscow. 1982.

[31] Höganäs. Somaloy Prototyping Material, SPM [Cited 14.04.2021] Available at: https://www.hoganas.com/globalassets/download-media/sharepoint/brochures-and-datasheets---all-documents/somaloy-prototyping-material_march_2016_1334hog.pdf

[32] F. Fiorillo and A. Novikov, "An improved approach to power losses in magnetic laminations under nonsinusoidal induction waveform," in IEEE Transactions on Magnetics, vol. 26, no. 5, pp. 2904-2910, Sept. 1990

[33] A. G. Kostyuk. Dynamics and strength of turbomachines: textbook for universities. 3rd ed. MPEI Publishing House. Moscow 2007.

[34] G.S. Samoilovich, B.M. Troyanovsky. Variable operation of steam turbines. Gosenergoizdat. Moscow, 1955.

[35] Rumyantsev M.Yu., Sizyakin A.V., Shevyrev N.I. Analysis of electromagnetic processes in high-speed electrical machines with foil gas-dynamic bearings // IEEE International Power Electronics and Motion Control Conference. 2016. Varna. pp. 530-536.

[36] Yu.N. Kalachev. Vector control (practice notes). [Cited 20.03.2020]. Available at: http://www.efo-power.ru/BROSHURES_CATALOGS/KALACHEV.pdf

Appendix 1. Calculation of a single-stream radial-axial stage

Defining parameters of the working fluid

Gas constant: $R := 287 \frac{J}{kg \cdot K}$

Adiabatic exponent: $k := 1.4$ $m_B := \frac{k-1}{k} = 0.286$

Specific heat capacity: $Cp := \frac{k}{k-1} \cdot R = 1.005 \cdot \frac{kJ}{kg \cdot K}$

Reference viscosity at 291,15K $\mu_0 := 1.827 \times 10^{-5} \frac{kg}{s \cdot m}$

Reference temperature for viscosity: $T_{00} := 291.15K$

Sutherland's constant: $C := 120K$

Setting static parameters for the calculation

Initial air temperature: $t'_0 := 28.8\,°C$

Initial air temperature in K: $T'_0 := t'_0 = 301.95\,K$

Initial static air pressure: $P'_0 := 2.6bar$

Network losses: $\zeta_c := 0.709062$

Barometric air pressure: $B := 101.325kPa$

Mass flow rate: $G := 0.03693831 \frac{kg}{s}$

Turbine inlet pipe diameter: $d_{pipe} := 25mm$

Turbine entry speed: $c_0 := \frac{G \cdot R \cdot T'_0}{\left(\frac{\pi \cdot d_{pipe}^2}{4}\right) \cdot P'_0} = 25.081 \cdot \frac{m}{s}$

Preliminary design values

Pressure after turbine: $P_B := \frac{B}{\zeta_c} = 142.9 \cdot kPa$

Enthalpy in front of the turbine: $h_0 := Cp \cdot T'_0 + \frac{c_0^2}{2} = 303.623 \cdot \frac{kJ}{kg}$

Full pressure in front of the turbine: $P_0 := 2.6102bar$

Full temperature in front of the turbine $T_0 := \frac{h_0}{Cp} = 302.263\,K$

Expansion ratio in turbine: $\delta := \frac{P_0}{P_B} = 1.827$

Isoentropic expansion work in a turbine: $H_0 := Cp \cdot T_0 \cdot \left(1 - \delta^{-\frac{k-1}{k}}\right) = 48.012 \cdot \frac{kJ}{kg}$

Ideal turbine power: $N_0 := H_0 \cdot G = 1.773 \cdot kW$

Fictitious speed: $C_f := \sqrt{2 \cdot H_0} = 309.877 \cdot \frac{m}{s}$

Specified design ratios and coefficients

Nozzle speed coefficient $\varphi := 0.95$

Impeller speed coefficient $\psi := 0.85$

Angle of flow into the nozzle $\alpha_0 := 90°$

Angle of flow out of the nozzle apparatus $\alpha_1 := 10°$

Nozzle discharge coefficient $\mu_{v1} := 0.85$

Impeller discharge coefficient $\mu_{v2} := 0.85$

Rotor speed $n := 150000 \frac{rad}{min}$

Stage calculation

Let's set the angles and the necessary coefficients:

$\alpha_2 := 90°$ $\beta_1 := 90°$ $m := 1.3$ $\frac{d_1}{d_2} = m$

μ1 shows the ratio of the peripheral speed c1u to u1:

$$\mu_1 := \frac{1}{1 - \frac{\tan(\alpha_1)}{\tan(\beta_1)}} = 1$$

$$\mu_2 := m \cdot \mu_1 \cdot \tan(\alpha_1) \cdot \cot(\alpha_2) = 0$$

Optimal U/Cf=Xad for this configuration of turbine:

$$x_{ad} := \frac{\psi}{\sqrt{\left(\frac{\mu_1}{\varphi \cdot \cos(\alpha_1)}\right)^2 \cdot \left[(\varphi \cdot \sin(\alpha_1))^2 + \psi^2 \cdot \left(1 - \varphi^2\right)\right] + \left(\frac{1 - \mu_2}{m}\right)^2 + 2 \cdot \psi^2 \cdot \mu_1 - \left(\frac{\psi}{m}\right)^2}} = 0.648$$

Degree of reaction: $\rho := 1 - \left(\frac{\mu_1 \cdot x_{ad}}{\varphi \cdot \cos(\alpha_1)}\right)^2 = 0.52$

Peripheral speed at maximum diameter: $u_1 := x_{ad} \cdot \sqrt{2 \cdot H_0} = 154.455\,m \cdot \frac{m}{s}$

Peripheral diameter of the impeller: $d_1 := \frac{u_1}{\pi \cdot n} = 25.566 \cdot mm$

Heat drop per nozzle system: $H_c := H_0 \cdot (1 - \rho) = 23.031 \cdot \frac{kJ}{kg}$

Heat drop per impeller: $H_p := H_0 \cdot \rho = 24.981 \cdot \frac{kJ}{kg}$

Parameters in front of turbine (point 0 parameters):

$P_0 = 261.02 \cdot kPa$ $T_0 = 302.263\,K$ $V_0 := \frac{R \cdot T_0}{P_0} = 0.332\,\frac{m^3}{kg}$ $h_0 := Cp \cdot T_0 = 303.623 \cdot \frac{kJ}{kg}$

Parameters after nozzle system (point 1 parameters):

Expansion ratio for nozzle system: $\delta_c := \left(1 - \frac{H_c}{Cp \cdot T_0}\right)^{\frac{1}{-m_в}} = 1.318$

Pressure after nozzle system: $p_1 := \frac{P_0}{\delta_c} = 198.046 \cdot kPa$

Theoretical enthalpy after the nozzle system: $h_{1t} := h_0 - H_c = 280.592 \cdot \frac{kJ}{kg}$

Theoretical temperature after the nozzle system: $T_{1t} := \frac{h_{1t}}{Cp} = 279.335\,K$

Theoretical specific volume of air after the nozzle system:

$v_{1t} := \frac{R \cdot T_{1t}}{p_1} = 0.405 \frac{m^3}{kg}$

Theoretical speed from the nozzle system: $c_{1t} := \sqrt{2 \cdot H_c} = 165.093\,m \cdot \frac{m}{s}$

Theoretical Mach number: $M_{1t} := \frac{c_{1t}}{\sqrt{k \cdot R \cdot T_{1t}}} = 0.641$

Actual speed from the nozzle system: $c_1 := c_{1t} \cdot \varphi = 203.889 \frac{m}{}$

Actual enthalpy after the nozzle system: $h_1 := h_0 - \frac{c_1^2}{2} = 282.838 \cdot \frac{kJ}{kg}$

Losses in the nozzle system: $\Delta H_c := \frac{c_{1t}^2 - c_1^2}{2} = 2.246 \cdot \frac{kJ}{kg}$

Actual temperature after the nozzle system: $T_1 := \frac{h_1}{Cp} = 281.571\,K$

Actual specific volume after the nozzle system: $v_1 := \frac{R \cdot T_1}{p_1} = 0.408 \frac{m^3}{kg}$

Nozzle throat area: $F_1 := \frac{G \cdot v_{1t}}{\mu_1 \cdot c_{1t}} = 69.67 \cdot mm^2$

Impeller blade height at inlet: $l_1 := \frac{F_1}{\pi \cdot d_1 \cdot \sin(\alpha_1)} = 4.995 \cdot mm$

Impeller inlet area (for BladeGen): $F_{1disc} := \pi \cdot d_1 \cdot l_1 = 401.215 \cdot mm^2$

Relative speed of entry into the impeller:

$$w_1 := \sqrt{{c_1}^2 + {u_1}^2 - 2 \cdot c_1 \cdot u_1 \cdot \cos(\alpha_1)} = 27.235\,\text{m} \cdot \frac{\text{m}}{\text{s}}$$

Entrance angle to the impeller:

$$\beta_1 := \text{acos}\left(\frac{c_1 \cdot \cos(\alpha_1) - u_1}{w_1}\right) = 90 \cdot °$$

Enthalpy of complete deceleration in relative motion at the outlet of the nozzle system:

$$h_{1w} := h_1 + \frac{{w_1}^2}{2} = 283.465 \cdot \frac{\text{kJ}}{\text{kg}}$$

Parameters after impeller (point 2 parameters):

Theoretical enthalpy at the exit from the impeller:

$$h_{2t} := h_1 - Cp \cdot T_1 \cdot \left[1 - \left(\frac{p_1}{P_B}\right)^{-\frac{k-1}{k}}\right] = 257.657 \cdot \frac{\text{kJ}}{\text{kg}}$$

Theoretical temperature at the outlet of the impeller:

$$T_{2t} := \frac{h_{2t}}{Cp} = 256.503\,\text{K}$$

Theoretical specific volume at the outlet of the impeller:

$$v_{2t} := \frac{R \cdot T_{2t}}{P_B} = 0.515\,\frac{\text{m}^3}{\text{kg}}$$

Peripheral speed at the average exit diameter from the accepted ratio of diameters:

$$u_2 := \frac{u_1}{m} = 118.812\,\text{m} \cdot \frac{\text{m}}{\text{s}}$$

Thepretical and actual speed of exit from the impeller:

$$w_{2t} := \sqrt{{w_1}^2 + 2H_p + \left({u_2}^2 - {u_1}^2\right)} = 186.425\,\frac{\text{m}}{\text{s}} \qquad w_2 := w_{2t} \cdot \psi = 158.461\,\frac{\text{m}}{\text{s}}$$

Energy losses in the impeller:

$$\Delta H_p := \frac{{w_{2t}}^2 - {w_2}^2}{2} = 4.822 \cdot \frac{\text{kJ}}{\text{kg}}$$

Actual enthalpy behind the impeller:

$$h_2 := h_{1w} - \frac{{w_2}^2}{2} = 270.91 \cdot \frac{\text{kJ}}{\text{kg}}$$

Actual temperature behind the impller: $T_2 := \frac{h_2}{Cp} = 269.696\,K$

Actual specific volume behind the impeller: $v_2 := \frac{T_2 \cdot R}{P_B} = 0.542\,\frac{m^3}{kg}$

The ratio of the meridional projections of velocities and the angle of exit in relative motion.

$K_c = \frac{c_{2rm}}{c_{1rm}}$ $K_c := 1$ $\beta_2 := \operatorname{asin}\left[K_c \cdot \left(\frac{c_1 \cdot \sin(\alpha_1)}{w_2}\right)\right] = 12.911 \cdot °$

Absolute velocity and flow angle from impeller:

$c_2 := \sqrt{w_2^2 + u_2^2 - 2 \cdot w_2 \cdot u_2 \cdot \cos(\beta_2)} = 35.405\,\frac{m}{s}$ $\alpha_2 := \operatorname{acos}\left(\frac{w_2 \cdot \cos(\beta_2) - u_2}{c_2}\right) = 90 \cdot °$

Calculation of losses on blades and blade efficiency

Losses in nozzle system: $\Delta H_c := \frac{c_{1t}^2}{2} - \frac{c_1^2}{2} = 2.246 \cdot \frac{kJ}{kg}$

Losses in impeller: $\Delta H_p := \frac{(w_{2t})^2}{2} - \frac{w_2^2}{2} = 4.822 \cdot \frac{kJ}{kg}$

Losses with not used output speed: $\Delta H_{out} := \frac{(c_2)^2}{2} = 0.627 \cdot \frac{kJ}{kg}$

Blade efficiency: $\eta_{blade} := \frac{H_0 - \Delta H_c - \Delta H_p - \Delta H_{out}}{H_0} = 0.8397$

Discharge coefficient for nozzle system and impeller

$\mu_{n.a.} := \frac{c_1 \cdot v_1}{c_{1t} \cdot v_{1t}} = 0.958$ $\mu_{impeller.} := \frac{w_2 \cdot v_2}{w_{2t} \cdot v_{2t}} = 0.894$

Determination of geometric characteristics

Impeller exit area: $F_2 := \frac{G \cdot v_{2t}}{c_2 \cdot \sin(\alpha_2)} = 537.47 \cdot mm^2$

Blade to blade area in the impeller (for BladeGen): $F_{2\_b2b} := \frac{G \cdot v_{2t}}{w_2} = 120.087 \cdot mm^2$

Impeller outer diameter: $d_1 = 25.566 \cdot mm$

Average diameter of the impeller at the outlet: $d_2 := \frac{d_1}{m} = 19.666 \cdot mm$

Impeller outlet outer diameter: $d_{2out.perif} := \sqrt{d_2^2 + \frac{2F_2}{\pi}} = 26.998 \cdot mm$

Impeller outlet inner diameter $d_{2out.inner} := \sqrt{d_2^2 - \frac{2F_2}{\pi}} = 6.677 \cdot mm$

Height of the blade at the outlet of the impeller

$$l_2 := \frac{d_{2out.perif} - d_{2out.inner}}{2} = 10.161 \cdot mm$$

Stage calculation results

$d_1 = 25.566 \cdot mm$ $l_1 = 4.995 \cdot mm$ $\alpha_1 = 10 \cdot °$

$d_2 = 19.666 \cdot mm$ $d_{2out.perif} = 26.998 \cdot mm$ $d_{2out.inner} = 6.677 \cdot mm$ $\beta_2 = 12.911 \cdot °$

Calculation of additional losses

Gap losses:

Assume that gaps are: $\Delta_1 := 0.15mm$ $\Delta_2 := 0.15mm$

Losses in gaps: $\zeta_{gap} := \left(\frac{\frac{\Delta_1}{l_1}}{1 + \frac{\Delta_1}{l_1}} \right)^2 \cdot \rho + 0.45 \cdot \frac{\Delta_2}{l_2} \cdot \left(1 + \frac{1}{\frac{d_2}{l_2}} \right) = 0.011$

Friction losses:

Assume the clearance at the impeller end: $s := 0.5mm$

Viscosity in the gap: $\nu_{1t} := v_1 \cdot \mu_0 \cdot \frac{T_{00} + C}{T_1 + C} \cdot \left(\frac{T_1}{T_{00}} \right)^{\frac{3}{2}} = 7.259 \times 10^{-6} \frac{m^2}{s}$

Reynolds number in the gap: $Re_1 := \frac{\left(\frac{d_1}{2}\right)^2 \cdot (2 \cdot \pi \cdot n)}{\nu_{1t}} = 3.536 \times 10^5$

Coefficient: $k_1 := 0.07 \cdot \left(\frac{s}{\frac{d_1}{2}}\right)^{\frac{1}{10}} \cdot Re_1^{-\frac{1}{5}} = 3.932 \times 10^{-3}$

Disk friction losses: $\zeta_{disk} := k_1 \cdot \frac{d_1 \cdot x_{ad}^3}{\pi \cdot l_1 \cdot \sqrt{1-\rho} \cdot \sin(\alpha_1)} = 0.0145$

Relative efficiency and power

Efficiency of turbine unit: $\eta_{oi} := \eta_{blade} - \zeta_{disk} - \zeta_{gap} = 0.815$

Check for equality energy on turbine:

$Lu := u_1 \cdot c_1 \cdot \cos(\alpha_1) + u_2 \cdot c_2 \cdot \cos(\alpha_2) = 40.317 \cdot \frac{kJ}{kg}$

$Lu := 0.5 \cdot \left(c_1^2 - c_2^2 + w_2^2 - w_1^2 - u_2^2 + u_1^2\right) = 40.317 \cdot \frac{kJ}{kg}$

Internal heat drop: $H_i := H_0 \cdot \eta_{oi} = 39.117 \cdot \frac{kJ}{kg}$

Internal power: $N_i := H_i \cdot G = 1.445 \cdot kW$

Electrical power, if efficiency of generator is 0.8: $N := N_i \cdot 0.8 = 1.156 \cdot kW$

Calculation of the nozzle apparatus

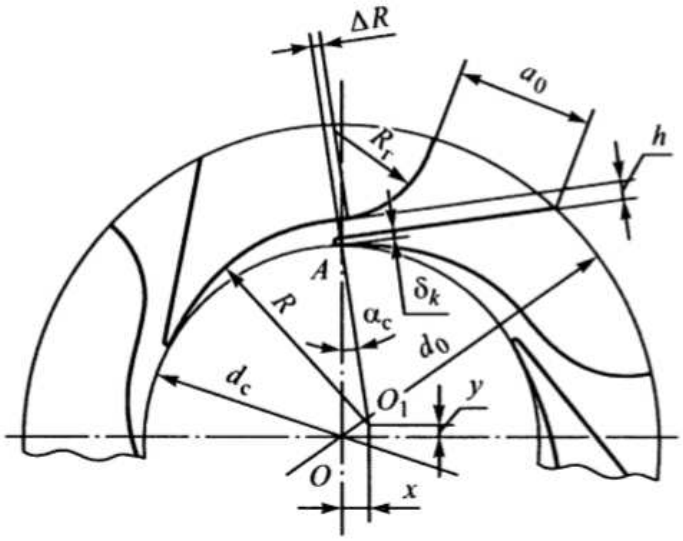

Number of channels: $z_c := 6$ $d_1 = 25.566 \cdot mm$

Height of channels: $l_1 := \frac{F_{1disc}}{(26.5mm) \cdot \pi} = 4.819 \cdot mm$

Inner diameter for nozzle apparatus: $d_1 := d_1 + 1mm = 26.566 \cdot mm$ $r_1 := \frac{d_1}{2} = 13.283 \cdot mm$

Channel throad width: $h_1 := \frac{F_1}{6 \cdot l_1} = 2.409 \cdot mm$

Average angle of flow: $\alpha_{1cp} := \operatorname{asin}\left[\frac{\frac{F_1}{\left(\frac{d_1}{2}\right)^2}}{\left(\frac{2 \cdot \pi \cdot l_1}{\frac{d_1}{2}}\right)}\right] = 9.975 \cdot °$

Assume this values: $\Delta := 1mm$ $\Delta R := 2mm$

Channel radius:

$$R := \frac{(h_1 + \Delta)^2 + 2 \cdot r_1 \cdot (h_1 + \Delta) \cdot \cos\left(\frac{2 \cdot \pi}{z_c} + \alpha_{1cp}\right) + r_1^2}{2 \cdot \left(h_1 + \Delta + r_1 \cdot \cos\left(\frac{2 \cdot \pi}{z_c} + \alpha_{1cp}\right)\right)} = 13.765 \cdot mm$$

Appendix 2. Calculation of a permanent magnet synchronous generator

Given parameters

Internal turbine power: $P' := 1.400\,kW$

Iterative coefficient Ke (E/U): $k_E := 1.015$

Loss factor due to waveform distortio: $k_\pi := 1.03$

Power conversion factor: $k_p := 1.12$

Efficiency of the DC / AC converter: $\eta_{elc} := 0.95$

Voltage drop across transistors: $\Delta U_t := 3V$

Phase number: $m_p := 3$

Power factor: $\cos\_\varphi := 1$

Number of pole pairs: $p := 1$

Rotation speed: $n := 150000\,\frac{rad}{min}$

Recalculation of voltages

Voltage of DC bus: $U_d := 620V$

$U_{ll\_m} := U_d \cdot \frac{\pi}{3} = 649.262\,V$ $\quad U_{phase\_m} := \frac{U_{ll\_m}}{\sqrt{3}} = 374.852\,V$

Winding voltages:

$U_{ll\_g} := \frac{U_{ll\_m}}{\sqrt{2}} = 459.098\,V$ $\quad U_{phase\_g} := \frac{U_{phase\_m}}{\sqrt{2}} = 265.06\,V$

Number of pulses: $m_{1\_pulses} := 6$

Recalculation of powers

Estimated generator power: $P' = 1.4 \cdot kW$

Power at generator terminals: $P_{alt} := \frac{P'}{k_E \cdot k_п} = 1.339 \cdot kW$

Power after rectifier: $P_d := \frac{P_{alt} \cdot U_d}{k_p \cdot (U_d + 2 \cdot \Delta U_t)} = 1.184 \cdot kW$

Power after inverter (On load): $P_{electric} := P_d \cdot \eta_{elc} = 1.125 \cdot kW$

Determination of the main dimensions

Current frequency $f := \frac{n}{p} = 2500 \cdot Hz$

Nominal phase current: $I_n := \frac{P_{alt}}{m_p \cdot U_{phase\_g}} = 1.684 \cdot A$

Linear current density: $A_\delta := 250 \frac{A}{cm}$

Assume flux density in air gap: $B_\delta := 0.54T$

Check the ratio A/B: $\frac{A_\delta}{B_\delta} = 46296.296 \frac{A}{m} \cdot \frac{1}{T}$ is less then 500 (A/cm)/T

Emperical pole overlap design factor: $\alpha_i := 0.635$

Form factor of the field Kf for sinusoidal pole $K_f := 1.11$

Shortening factor Kshort: $K_{short} := \sin\left(\frac{5}{6} \cdot \frac{\pi}{2}\right) = 0.966$

Number of slots per pole and phase: $q := 2$

Distribution coefficient: $K_{dist} := \frac{\sin\left(\frac{\pi}{2 \cdot m_p}\right)}{q \cdot \sin\left(\frac{\pi}{2 \cdot q \cdot m_p}\right)} = 0.966$

Skewness coefficient: $K_s := 1$

Winding coefficient: $K_w := K_s \cdot K_{short} \cdot K_{dist} = 0.933$

Lenght to diameter ratio: $\lambda_i := 3$

Rotor diameter: $D_r := \sqrt[3]{\frac{6.1 \cdot P'}{\alpha_i \cdot K_f \cdot K_w \cdot B_\delta \cdot A_\delta \cdot \lambda_i \cdot n \cdot 60}} = 12.882 \cdot mm \quad D_r := 13mm$

Rotor lenght: $l := \lambda_i \cdot D_r = 39 \cdot mm \quad l := 40mm$

Assume air gap lenght: $\delta := 1mm$

Bandage thickness: $\Delta b := 1.5mm$

Stator internal diameter: $D := D_r + 2 \cdot \Delta b + 2 \cdot \delta = 18 \cdot mm$

Stator pole pitch: $\tau := \frac{\pi \cdot D}{2 \cdot p} = 28.274 \cdot mm$

Calculation of the stator winding, slots and yoke

Magnetic flux: $\Phi_\delta := B_\delta \cdot l \cdot \tau \cdot \alpha_i = 3.878 \times 10^{-4} \cdot Wb$

Number of turns in a winding phase: $w_{phase} := \frac{k_E \cdot U_{phase\_g}}{4 \cdot K_f \cdot K_w \cdot f \cdot \Phi_\delta} = 66.985 \quad w_{phase} := 68$

Number of parallel winding branches: $a_1 := 1$

Number of parallel winding wires: $a_2 := 1$

Number of wires in slot: $u_{slot} := \frac{a_1 \cdot a_2 \cdot w_{phase}}{p \cdot q} = 34$

Number of teeth: $z := q \cdot 2 \cdot p \cdot m_p = 12$

Number of coils per phase $\frac{z}{m_p} = 4$

Toothed division: $t_z := \pi \cdot \frac{D}{z} = 4.712 \cdot mm$

Steel filling factor of the magnetic core section (steel 2421, GOS' $k_{fill} := 0.89$

Displacement flow ratio $\gamma_b := 0.93$

Allowable values of flux density in the tooth of steel 2421: $B_{z.max} := 1.2T$

Minimum tooth width: $b_{z.min} := \frac{B_\delta \cdot \pi \cdot D}{B_{z.max} \cdot k_{fill} \cdot z} = 2.383 \cdot mm$

If b.z.min <2mm, then we take 2mm

Wedge height $h_{wedge} := 0.5mm$

Cone height: $h_{cone} := 0.5mm$

Crown height: $h_{crown} := h_{wedge} + h_{cone} = 1 \cdot mm$

Allowable slot opening: $b_{allowable\_slot\_opening} := \frac{\pi \cdot \left(D + h_{crown} \cdot 2\right)}{z} - b_{z.min} = 2.853 \cdot mm$

Allowable current density: $j_a := 12 \frac{A}{mm^2}$

Wind cross-section: $S_a := \frac{I_n}{j_a \cdot a_1 \cdot a_2} = 0.14 \cdot mm^2$

Winding diameter (round to the closest standard value):

$d_a := \sqrt{\frac{S_a \cdot 4}{\pi}} = 0.423 \cdot mm$ $d_{av} := 0.5mm$ $S_{av} := \frac{d_a^2 \cdot \pi}{4} = 0.196 \cdot mm^2$

Slot utilization ratio: $k_{s.u.} := 0.35$

Cross-sectional area of the slot: $S_s := \frac{u_{slot} \cdot S_a}{k_{s.u.}} = 19.074 \cdot mm^2$

Height and width of the slot through trapezoidal area of a slot:

$h_s := 0 \quad b_{s.max} := 0$ Given

$$S_s = \frac{h_s \cdot \left(b_{allowable\_slot\_opening} + b_{s.max}\right)}{2} \quad \frac{\left(-b_{allowable\_slot\_opening} + b_{s.max}\right)}{2 \cdot \sin(15°)} = \frac{h_s}{\sin(75°)}$$

$$\begin{pmatrix} h_{sv} \\ b_{s.max} \end{pmatrix} := \text{Find}\left(h_s, b_{s.max}\right) = \begin{pmatrix} 4.652 \\ 5.346 \end{pmatrix} \cdot mm$$

Slot width: $b_s := \frac{b_{allowable\_slot\_opening} + b_{s.max}}{2} = 4.1 \cdot mm$

Coefficient for calculating the slot openning $\Delta b_{op} := 0.46mm$

Slot openning: $b_{slot\_opening} := d_a + \Delta b_{op} = 0.96 \cdot mm$

The pitch of the slot winding expressed by the number of slot divisi $y_п := m_p \cdot q = 6$

Average section width: $\tau_y := \frac{\pi \cdot \left(D - b_s\right) \cdot y_п}{z} = 21.834 \cdot mm$

Coefficients K1 and K2 to get length: $K_1 := 1.2 \quad K_2 := 0.26$

Average end winding length: $l_s := K_1 \cdot \tau_y + 1cm = 36.201 \cdot mm$

Average length of a coil of a section $l_{coil.avg} := \left(l + l_s\right) \cdot 2 = 152.402 \cdot mm$

Total length of the winding: $l_{coil.tot} := l_{coil.avg} \cdot w_{phase} = 10.363\,m \quad n_2 := 10$

Current displacement ratio $\gamma_a := 1 + \frac{n_2^{\,2} - 0.2}{15.25 \cdot \left(1 + \frac{l_s}{l}\right)} \cdot \left(d_a \cdot \frac{100}{m}\right)^4 \cdot \left(\frac{f}{50Hz}\right)^2 = 1.054$

Allowable overheating over 20 degrees: $\Delta\theta := 100\,°C$

Copper temperature coefficient of resistan $\alpha_\theta := 0.004 \cdot \frac{1}{K}$

Ohmic resistance of the armature winding phase:

$$r := \frac{l_{coil.avg} \cdot w_{phase} \cdot \left[1 + \alpha_\theta \cdot (\Delta\theta - 273.15K)\right]}{57000000 \cdot \left(\frac{1}{m \cdot \Omega}\right) \cdot S_a \cdot a_1 \cdot a_2} = 1.296\,\Omega \qquad r_a := r \cdot \gamma_a = 1.366 \cdot \Omega$$

$$\beta := \frac{y_\Pi}{z \cdot 0.5} = 1 \qquad k_{1\beta} := 0.25 \cdot (1 + 3 \cdot \beta) = 1 \qquad k_\beta := 0.25 \cdot \left(1 + 3 \cdot k_{1\beta}\right) = 1 \qquad \Delta h := 2mm$$

Slot permeance:

$$left := \frac{h_s + h_{crown} - \left(\Delta h + h_{wedge} + h_{cone}\right)}{3 \cdot b_s} \cdot k_\beta$$

$$right := \left(\frac{\Delta h}{2 \cdot b_s} + \frac{3 \cdot h_{cone}}{b_s + 2 \cdot b_{slot\_opening}} + \frac{h_{wedge}}{b_{slot\_opening}}\right) \cdot k_{1\beta}$$

$$\lambda_{slot} := 0.4\pi \cdot (left + right) = 1.545$$

Permeance through tooth crown: $\lambda_t := 1.25 \cdot 5 \cdot \frac{\delta}{\left(5 \cdot b_{slot\_opening} + 4 \cdot \delta\right)} = 0.71$

Differential scattering $\sigma\delta k_{o2} := 0.0265$

$$\lambda_d := 0.2 \cdot \frac{\tau}{\pi \cdot \delta} \cdot \frac{z}{p} \cdot \sigma\delta k_{o2} = 0.572$$

Specific permeance around end windin $\lambda_{end} := 0.42 \cdot \frac{q}{l} \cdot \left(l_s - 0.64 \cdot \beta \cdot \tau\right) = 0.38$

Total specific permeance: $\lambda_s := \lambda_{slot} + \lambda_t + \lambda_d + \lambda_{end} = 3.208$

Leakage inductive resistance: $X_s := 1.26 \cdot 100 \cdot f \cdot \frac{w_{phase}^2}{p \cdot q} \cdot l \cdot \lambda_s \cdot 10^{-7} \cdot \frac{s \cdot \Omega}{m} = 9.345\,\Omega$

Internal EMF of the armature at rated load:

$$E_i := \sqrt{\left(U_{phase\_g} \cdot \cos\_\varphi + I_n \cdot r_a\right)^2 + \left[U_{phase\_g} \cdot (1 - \cos\_\varphi)^2 + I_n \cdot X_s\right]^2} = 267.823 \cdot V$$

$$k_E := \frac{E_i}{U_{phase\_g}} = 1.01$$

Refined magnetic flux value: $\Phi_\delta := \frac{E_i}{4 \cdot K_f \cdot K_w \cdot f \cdot w_{phase}} = 3.803 \times 10^{-4} \cdot Wb$

Permissible value of flux density in steel: $B_{ja} := 1.2T$

Anchor back radial height: $h_{ja} := \frac{\Phi_\delta}{2 \cdot (l) \cdot k_{fill} \cdot B_{ja}} = 4.451 \cdot mm$

Stator diameter $D_H := D + 2 \cdot \left(h_s + h_{crown}\right) + 2 \cdot h_{ja} = 38.207 \cdot mm$